

# The Angular Correlation Function and Hierarchical Moments of $\sim 70000$ Faint Galaxies to $R=23.5$

Nathan Roche<sup>1,2</sup> and Stephen A. Eales<sup>1,3</sup>

<sup>1</sup>*Department of Physics and Astronomy, University of Wales Cardiff, P.O. Box 913, Cardiff CF2 3YB*

<sup>2</sup>*ndr@astro.cf.ac.uk*

<sup>3</sup>*S.Eales@astro.cf.ac.uk*

5 February 2020

## ABSTRACT

We investigate the angular correlation function,  $\omega(\theta)$ , and third and fourth-order hierarchical moments of a large sample of  $\sim 70000$  faint galaxies with an estimated completeness limit of  $R = 23.5$ . The data, obtained using the new INT Wide Field Camera, consists of 47 red-band CCD images on two widely separated fields of areas  $1.01 \text{ deg}^2$  and  $0.74 \text{ deg}^2$ . Galaxy clustering is detected with a total significance of  $\sim 10\sigma$ . The angular correlation function at  $\theta > 5 \text{ arcsec}$  appears consistent with a  $\theta^{-0.8}$  power-law, with no flattening between limits of  $R = 21$  and  $R = 23.5$ . The  $\omega(\theta)$  amplitudes support the relatively high normalization of the Infante and Pritchet (1995) and Woods and Fahlman (1997)  $\omega(\theta)$  scaling, and are more consistent with stable clustering ( $\epsilon = 0$ ) than with models in which galaxy clustering was weaker in the past ( $\epsilon \sim 1.2$ ). Assuming the redshift distribution from our pure luminosity evolution model and the present-day galaxy correlation radii from Loveday et al. (1995), we estimate the clustering evolution as  $\epsilon = -0.03 \pm 0.44$ .

On the larger of our fields, the amplitude of  $\omega(\theta)$  is significantly higher at  $2 \leq \theta \leq 5 \text{ arcsec}$  than at  $\theta > 5 \text{ arcsec}$ , indicating an excess of physically close ( $< 20h^{-1} \text{ Mpc}$ ) galaxy pairs above the number expected from chance and from the clustering seen at larger scales. The fraction of galaxies which lie in excess close pairs increases between  $R = 21$  and  $R = 23$  limits, and is consistent with the number of close galaxy pairs seen locally combined with a merger/interaction rate evolving as  $(1+z)^m$  with  $m = 1.65^{+0.62}_{-0.88}$ .

We also estimate the hierarchical moments  $s_3(\theta)$  and  $s_4(\theta)$  from the galaxy counts-in-cells. For  $19 \leq R \leq 23.5$  galaxies,  $s_3(\theta)$  and  $s_4(\theta)$  are very similar to those measured from the APM and EDSGCS surveys at the shallower limit of  $B \leq 20$ . The evolution of  $s_3(\theta)$  is no more than  $\sim \pm 15\%$  between these magnitude limits. This implies that the rest-frame blue-band luminosity from galaxies continues to trace the underlying mass distribution, without strong linear or non-linear biasing, out to  $z \sim 1$ . The hierarchical moments support the interpretation of the stable clustering and moderate evolution of the merger rate as evidence for a low  $\Omega$  Universe with unbiased galaxies.

## Key words:

surveys – galaxies: clusters: general – galaxies: evolution – large-scale structure of Universe

## 1 INTRODUCTION

The clustering of galaxies on the sky is most often described in terms of the angular correlation function,  $\omega(\theta)$ , a projection onto the sky plane of the three-dimensional two-point correlation function  $\xi(r)$ . For galaxies of separation  $r$  in proper co-ordinates, at redshift  $z$ , the two-point correlation function is often parameterized as

$$\xi(r, z) = \left(\frac{r}{r_0}\right)^{-\gamma} (1+z)^{-(3+\epsilon)} \quad (1)$$

where  $r_0$  is the correlation radius,  $\gamma$  the slope, and  $\epsilon$  parameterizes the evolution of clustering (clustering stable in proper co-ordinates being  $\epsilon = 0$ ). The angular correlation function will be a power-law of slope  $\theta^{-(\gamma-1)}$  and amplitude given by the Limber's formula (e.g. Phillipps et al. 1978) integration of  $\xi(r, z)$  over the galaxy redshift distribution  $N(z)$ .

Photographic galaxy surveys indicated that  $\omega(\theta) \propto \theta^{-0.8}$  approximately, with a break at very large scales, and an amplitude which decreases with increasing depth, due to the effects of projection (e.g. Groth and Peebles 1977; Maddox et al. 1990). During the early 1990s, it was found from a number of CCD surveys that the  $\omega(\theta)$  amplitude of faint ( $B > 23.5$ ) galaxies falls well below the scaling predicted for stable clustering and a galaxy  $N(z)$  given by a non-evolving model (e.g. Efstathiou et al. 1991; Roche et al. 1993). This was interpreted (Roche et al. 1993, 1996) as evidence that  $N(z)$  at these magnitudes is more extended than the non-evolving prediction, implying an evolutionary brightening of  $L \sim L^*$  galaxies at higher redshifts. Alternatively, it could mean that the clustering of galaxies evolves rapidly (i.e.  $\epsilon \geq 1$ ) and so was much weaker at even moderate redshifts. Another possibility was that the faint blue galaxies at  $B > 23$  were a new population of blue dwarf galaxies at moderate redshifts, with much weaker clustering than  $L \sim L^*$  spirals (Babul and Rees 1992; Efstathiou 1995).

It was then found that the redder galaxies at these magnitudes gave a much ( $\sim 0.5$  dex) higher  $\omega(\theta)$  amplitude than the bluer galaxies (Neuschaefer et al. 1995; Roche et al. 1996). This would argue against a strong evolution of galaxy clustering as an explanation of the low  $\omega(\theta)$  amplitudes, but would be consistent with  $L^*$  evolution models, where the extended tail of  $N(z)$  would consist of blue star-forming giant galaxies. However, it would also be consistent with intrinsically weakly clustered blue dwarf galaxies at lower redshift.

Soon afterwards, the importance of  $L^*$  evolution was established directly when deeper redshift surveys with the Keck telescope (e.g. Cowie, Songaila and Hu 1996; Steidel et al. 1996) and Hubble Deep Field photometry (e.g. Madau et al. 1996; Bershadsky et al. 1997) identified many galaxies at  $z \sim 1-3$  and confirmed there is a brightening of the galaxy  $L^*$  at these redshifts.

As the luminosity evolution is becoming better determined by other data, the emphasis of studying faint galaxy clustering is changing from the use of  $\omega(\theta)$  as a probe of  $N(z)$  towards a more detailed investigation of the evolution of clustering and large-scale structure, the clustering properties of different types of galaxy, and the possible effects of interactions between galaxies. In particular, there is still much to learn about the rate of clustering evolution,  $\epsilon$ , which is sensitive to the cosmological parameters and also to any biasing of the luminosity distribution relative to the underlying mass distribution. Models (e.g. Colín, Carlberg and Couchman 1997) and direct observations from redshift surveys (e.g. Le Fèvre et al. 1996; Shepherd, Carlberg and Yee 1997; Carlberg et al. 1997) generally span a wide range of at least  $0 \leq \epsilon \leq 1.5$ , although models in which the bias factor increases rapidly with redshift (e.g. Matarrese et al. 1997) may predict galaxy clustering evolution closer to a comoving model with  $\epsilon = \gamma - 3 \simeq -1.2$ .

The first deep CCD surveys covered small ( $< 0.1 \text{ deg}^2$ ) areas of sky, on which the detection of galaxy clustering was only  $\sim 3\sigma$ , but with large format CCDs, such as the Wide Field Camera installed on the Isaac Newton Telescope last year, it becomes possible to survey  $> 1 \text{ deg}^2$  areas and study faint galaxy clustering in more detail. In this paper we present a study of galaxy clustering to a limit  $R = 23.5$  on two fields with total areas  $1.01 \text{ deg}^2$  and  $0.74 \text{ deg}^2$ . The larger fields will greatly reduce the ‘integral constraint’ cor-

rection (see Section 4), and the increase in sample size will provide better constraints on the clustering evolution.

Previous, less deep, surveys suggest that  $> 1 \text{ deg}^2$  areas can provide more than just the  $\omega(\theta)$  amplitude. Infante and Pritchet (1995), studying galaxy clustering to  $R \simeq 23$  on a  $2 \text{ deg}^2$  mosaic of photographic plates, reported a flattening of the slope of  $\omega(\theta)$  on going faintward. Infante, de Mello and Mentaneau (1996), on a similar area of short-exposure CCD images, found the  $\omega(\theta)$  amplitude of  $R < 21.5$  galaxies to be higher at  $2 < \theta < 6 \text{ arcsec}$  than at larger scales. This excess of close pairs of galaxies is caused by physical interactions and mergers, and its detection in deeper surveys would be important as there is currently much interest in the evolution of the merger rate.

With a large area, it may also be possible to measure the higher-order correlations functions, which are related to the higher-order moments (skewness, kurtosis etc.) of the galaxy counts-in-cells, in the same way that  $\omega(\theta)$  is related to the variance. These statistics provide additional information on the nature of galaxy clustering but until now have been studied only at much shallower limits (Gaztañaga 1994; Szapudi, Meiksin and Nichol 1996).

We assume  $H_0 = 50 \text{ km s}^{-1} \text{ Mpc}^{-1}$  and  $q_0 = 0.05$  throughout, but give some quantities in units of  $h = H_0/100 \text{ km s}^{-1} \text{ Mpc}^{-1}$ . In Section 2 of this paper we describe the observational data and its reduction and calibration, and in Section 3 the number counts of the galaxies and stars. Section 4 describes the analysis of the galaxy  $\omega(\theta)$ , and Section 5 presents the results. Section 6 describes models of galaxy evolution and clustering and compares these with our observations and other data. In Section 7 we discuss  $\omega(\theta)$  at small scales of a few arcsec and its use in investigating merger rate evolution. In Section 8 we investigate the higher-order moments of the sample and compare with results from less deep surveys. Section 9 discusses the implications of all these results in detail, and we summarize the main conclusions in Section 10.

## 2 DATA

### 2.1 Observations

Our data were acquired on the nights of 4th and 5th June 1997, on a service run of the recently installed Wide Field Camera (WFC), at the prime focus of the 2.5 metre Isaac Newton Telescope on La Palma. At that time the WFC was fitted with a  $2 \times 2$  array of Loral CCDs, each with  $2048 \times 2048$  pixels. In this configuration the pixel size corresponds to  $0.37 \text{ arcsec}$ . The WFC should then have provided a total area of approximately  $638 \text{ arcmin}^2$  with each pointing, but one of the four CCD chips was nonfunctional and another suffered a severe loss of sensitivity towards the edges, reducing the usable area to  $\sim 440 \text{ arcmin}^2$ . The WFC imaged 21 positions, 12 arranged in a  $3 \times 4$  grid referred to as field ‘e’, and 9 in a  $3 \times 3$  grid referred to field ‘f’. Field ‘e’ is centred at R.A. 14:00 hours, declination zero, which is galactic longitude  $337.01^\circ$  and latitude  $+58.26^\circ$ , and field ‘f’ is centred at R.A. 21:00 hours, declination  $-10^\circ$ , which is galactic longitude  $38.71^\circ$  and latitude  $-33.06^\circ$ . Each of the 21 pointings was exposed twice for 900 seconds, with the WFC Harris Red filter. For photometric calibration, 5 second exposures

**Table 1.** Positions (equinox 2000.0) of the 16 pointings of the WFC and estimates of the resolution on the images

Field name	R.A.	Dec.	FWHM (arcsec)
e1	14:00:00.00	+00:00:00.3	1.43
e2	13:59:59.98	+00:25:39.9	1.41
e4	14:00:00.00	-00:51:19.7	1.51
e7	14:01:38.05	+00:00:00.3	1.70
e8	14:01:37.94	-00:24:29.7	1.73
e9	14:01:37.84	-00:49:01.3	1.62
e10	13:58:22.10	-00:00:00.1	1.51
e11	13:58:22.07	+00:24:29.3	1.63
e12	14:01:38.16	+00:24:29.3	1.88
f1	21:00:00.09	-10:00:00.2	1.92
f2	20:59:59.97	-10:24:29.9	1.89
f4	21:01:39.00	-09:35:29.8	1.72
f6	21:01:38.98	-10:24:25.7	2.19
f7	20:58:21.07	-09:35:29.2	1.68
f8	20:58:21.01	-09:59:58.5	1.55
f9	20:58:21.03	-10:24:28.7	1.78

were taken of several fields containing standard stars from the catalog of Landolt (1992).

Some further sections of the data were rendered unusable by autoguider malfunctions and a period of poor seeing. We were able to use a total of 47 CCD frames (27 in field ‘e’ and 20 in field ‘f’) from 16 pointings of the WFC at coordinates given in Table 1.

## 2.2 Reduction and source detection

The initial processing of the data was carried out using IRAF. For each of the three functional CCD chips, a bias frame was produced and subtracted from all images. One of the three CCD chips showed a significant falloff in sensitivity towards the edges. We trimmed these images approximately where the sensitivity fell to 0.64 of its central value, reducing the area by  $\sim 25\%$ . For each chip, median flat fields were generated from the data using IRAF ‘ccdcombine’, by taking the median of all 32 exposures on the positions in Table 1, rejecting those pixels containing bright objects. All images were then divided by the respective normalized flat fields.

The two exposures at each position were added using IRAF ‘ccdcombine’, using the ‘crrrej’ option (rejecting the higher of the two values if discrepant by  $> 3\sigma$ ) to remove the majority of cosmic rays. KAPPA ‘surfit’ was used to fitting high-order spline surfaces to the sky background on each image, which were subtracted from the data. Images in the ‘f’ field suffered from small-scale variations in sky background much more than those in the ‘e’ field, at least in part as a result of the greater number of bright stars in field ‘f’. The mean sky background intensity (using the calibration in Section 2.3) was  $20.77 \pm 0.02 R \text{ mag arcsec}^{-2}$  on field ‘e’ and  $20.70 \pm 0.02 R \text{ mag arcsec}^{-2}$  on field ‘f’.

The Starlink PISA (Position, Intensity and Shape Analysis) package, developed by M. Irwin, P. Draper and N. Eaton, was used to detect and catalog the objects, with the chosen detection criterion that a source must exceed an intensity threshold of  $1.5\sigma$  above the background noise ( $\sigma$  being separately determined by PISA for each image) in at least 6 connected pixels. The mean detection threshold was  $25.72 \pm 0.01 R \text{ mag arcsec}^{-2}$  on field ‘e’ and  $25.63 \pm 0.02 R$

$\text{mag arcsec}^{-2}$  on field ‘f’. PISA was run with deblend (objects connected at the detection threshold may be split if they are separate at a higher threshold) and the ‘total magnitudes’ option, which estimates total intensity above the background by fitting an elliptical aperture to each individual detection and performing a ‘curve-of-growth’ analysis.

We excluded data from circular ‘holes’ (radius 15 to 100 arcsec) around many of the bright, saturated stellar images in order to remove spurious noise detections. Radial profiles were fitted to several non-saturated stars on each image using ‘pisaft’, giving the FWHM estimates listed in Table 1. It is evident that the seeing was less than ideal during the period of observation, resulting in a FWHM averaging  $1.60 \pm 0.04 \text{ arcsec}$  on field ‘e’ and  $1.82 \pm 0.07 \text{ arcsec}$  on field ‘f’, with much variation between the individual images.

Star-galaxy separation was performed using plots of central against total intensity, normalized to the ratio from the fitted stellar profile. The stellar locus could be separated from the galaxies only to  $R \sim 21$ , so fainter objects are assumed to be galaxies, but we later (Sections 3 and 5) apply corrections to our results for the effects of faint star contamination. The number counts of objects classed as stars and galaxies are compared in Section 3.

## 2.3 Calibration

For the purposes of photometric calibration, we interspersed the 900s exposures with short exposures of three fields containing standard stars (about 5 per CCD chip per field) from Landolt (1992). After flat-fielding the standard star images, all the catalogued stars were identified, and their intensities measured using PISA.

For each observation of a standard star, the photon count rate  $C$  will relate to the catalogued red magnitude  $R$  and colour  $V - R$  as

$$2.5 \log(C) = R + r_1 + r_2 X + r_3 (V - R) \quad (2)$$

where  $r_1$  is the zero-point outside the atmosphere,  $r_2$  is the atmospheric extinction at the zenith,  $X$  is the airmass of each observation and  $r_3$  is a colour-correction term expressing the difference between our passband and the Cousins  $R$  band of Landolt (1992). The standard star observations were too few in number and covered too small a range of airmass to accurately measure  $r_2$ , so instead we estimated  $r_2$  by integrating a tabulated measurement of the extinction curve at La Palma over the  $R$  passband. Assuming a  $f_\nu \propto \nu^{-1}$  source gave  $r_2 = 0.062$ .

We derive separate photometric calibrations for each of the three CCD chips. The colour term  $r_3$  was consistent with zero within the statistical errors, so we simply fit

$$2.5 \log(C) = R + r_1 + 0.062X \quad (3)$$

to the standard star observations, which gave  $r_1 = -32.571 \pm 0.012$ ,  $-32.521 \pm 0.005$  and  $-32.754 \pm 0.004$  for the three CCD chips. The photon counts for each detection could then be converted to  $R$  magnitudes at the zenith with

$$R = -2.5 \log(C) - (r_1 + 0.062X) \quad (4)$$

appropriate to the chip and airmass of observation.

The HI survey map of Stark et al. (1992) gives the Galactic HI column  $N_H$  as  $2.7 \times 10^{20} \text{ cm}^{-2}$  on field ‘e’ and  $4.9 \times 10^{20} \text{ cm}^{-2}$  on field ‘f’. From the Burstein and Helles

(1978) relation of Galactic dust reddening to  $N_H$ , this implies negligible reddening on field ‘e’ but  $E(B - V) \simeq 0.04$  mag on field ‘f’, corresponding to  $R$ -band extinction of approximately 0.10 mag. A Galactic extinction correction  $\Delta(R) = -0.10$  was then applied to the magnitudes from the ‘f’ field.

## 2.4 Astrometry

To derive astrometric transforms, we made use of the APM database at the Institute of Astronomy in Cambridge. Field ‘e’ lay within the measured UKST plate F865 and field ‘f’ within the measured UKST plate F742. We identified 12 catalogued stars on each of the 47 CCD images, and using their R.A. and Dec. fitted astrometric transforms using the IRAF ‘*pltsol*’ routine. The residuals in these fits average only 0.5 arcsec RMS. The pixel co-ordinates of all detections were then converted to R.A. and Dec. The catalogs of detections on the 47 individual images could then be combined into two composite catalogs for the ‘e’ and ‘f’ fields.

There are a number of regions where the areas of adjacent images overlapped by a few arcminutes. For all overlap areas, we matched together the two detections of the same objects and compared the measured magnitudes, thus estimating photometric scatter as  $\sigma(R) = 0.14$  mag for  $R < 22$  detections, 0.22 mag at  $22 < R < 23$  and 0.24 mag at  $23 < R < 24$ . In most overlap regions the mean difference between the magnitude measurements of the same objects was consistent with zero within  $2\sigma$ , but in a few cases there was a significant offset, presumably as a result of poor atmospheric conditions during acquisition of one of the images. In this way it was estimated that field e7 suffered a loss of  $0.18 \pm 0.06$  mag, field e8 a loss of  $0.41 \pm 0.09$  mag and f6 a loss of  $0.09 \pm 0.04$  mag relative the rest of the data. Estimated corrections of  $-0.18$ ,  $-0.41$  and  $-0.09$  mag were applied to magnitudes in the e7, e8 and f6 catalogs respectively. For the areas of overlap, we adopted the positions and magnitudes derived from the image with the better seeing (Table 1) when combining the detection catalogs. After taking into account the overlap regions and holes, the areas covered by usable data amount to  $1.012 \text{ deg}^2$  for field ‘e’ and  $0.740 \text{ deg}^2$  for field ‘f’.

## 3 GALAXY AND STAR COUNTS

Figure 1 shows the differential number counts of objects classed as galaxies on the ‘e’ and ‘f’ fields, together with galaxy counts from some previous CCD surveys in very similar passbands, and the PLE and non-evolving models described in Section 6. The error bars are derived from the scatter in the counts from the individual images making up each field (this will underestimate the true error by a factor of up to  $\sim 2$  as the images are adjacent rather than independent). Comparison of the galaxy counts with deeper data suggests our detection of galaxies is virtually complete to  $R = 23.5$ , but becomes significantly ( $\sim 30\%$  on field ‘e’,  $\sim 45\%$  on field ‘f’) incomplete at  $23.5 < R < 24$ , before the counts turn over at  $R > 24$ . As incompleteness can unpredictably affect measures of clustering, we limit our analysis to the  $R \leq 23.5$  galaxies.

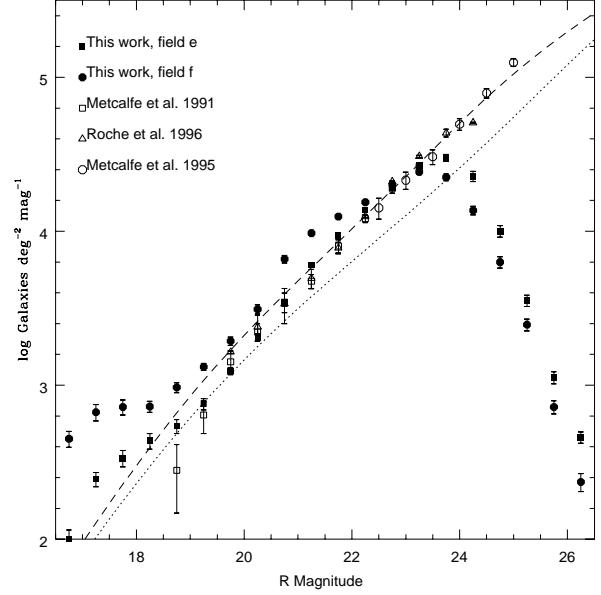


**Figure 1.** Differential galaxy number counts, in 0.5 mag intervals of  $R$  magnitude, for our two survey fields compared to previous CCD surveys in very similar passbands and the predictions of our PLE (dashed) and non-evolving (dotted) models.

To  $R \simeq 23.5$ , the field ‘e’ galaxy counts appear reasonably consistent with both previous observations and the PLE model. In contrast, the galaxy counts from field ‘f’ show significant excesses at  $R < 19$  and at  $20.5 < R < 22.5$ . This is undoubtedly the result of star contamination. The excess at  $R < 19$  is due to large numbers of bright, saturated stars becoming misclassified as galaxies. We simply exclude all 1543 of the  $R < 19$  objects on the ‘f’ field from the analysis, as it is estimated that only half will be real galaxies, and the loss of a few hundred galaxies ( $\sim 1\%$  of our sample) will not be significant. The star contamination at  $R > 20.5$  is a more serious problem. We were only able to separate stars from galaxies to  $R \sim 21$ , so there will inevitably be star-contamination at fainter magnitudes. We estimate this contamination using the star counts at  $R < 21$ .

Figure 2 shows the number counts of objects classed as stars. The star counts in the magnitude range  $18.0 < R < 20.5$  were fitted with power-laws, giving  $\log N_{stars} = 3.091 + 0.1557(R - 20.5)$  for field ‘e’ and  $\log N_{stars} = 3.502 + 0.1320(R - 20.5)$  for field ‘f’. The slopes are very similar but the normalization is 2.6 times higher for field ‘f’, due to its lower Galactic latitude. Faintward of  $R \sim 20-21$ , star counts flatten and approach the  $\gamma \simeq 0.04$  slope of the stellar luminosity function (Bahcall and Soneira 1980). The models used by Couch, Jurčević and Boyle (1993) to correct for stellar contamination incorporate star-count gradients of  $\gamma \simeq 0.05-0.06$  at  $R \simeq 21-23$ . We estimate the faint-star contamination of our galaxy catalog by (i) assuming stars are classified correctly to  $R = 20.5$  (ii) estimating the number of  $R > 20.5$  stars by extrapolating the fitted power-laws with  $\gamma = 0.05$  at  $R > 20.5$  (as shown on the plot). The number of contaminating stars on each field is then estimated as the summation of the extrapolated star-counts from  $R = 20.5$

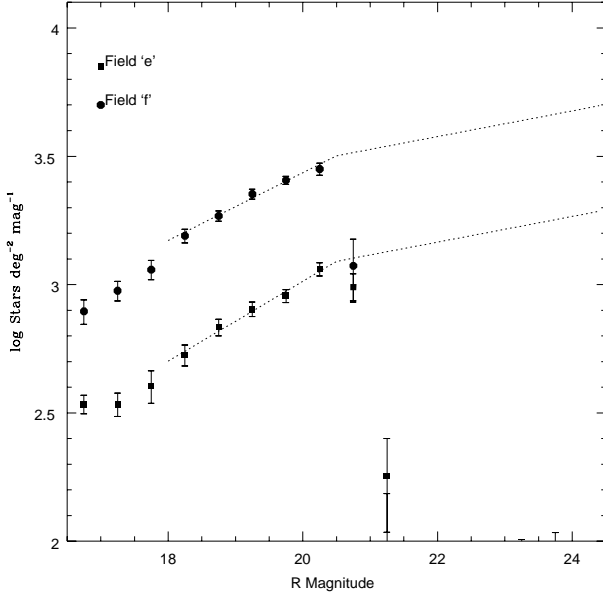


**Figure 2.** Differential star number counts in 0.5 mag intervals of  $R$  magnitude, with the power-laws fitted at  $18 < R < 20.5$  (dashed lines) and their extrapolations with  $\gamma = 0.05$  slopes at  $R > 20.5$ .

to the magnitude limit being considered, minus the number of  $R > 20.5$  detections already classified as stars.

In this way, we estimate that about 3382 of the 42673 objects classed as  $R \leq 23.5$  galaxies on field ‘e’, and about 7945 of the 35149 objects classed as  $19.0 \leq R \leq 23.5$  galaxies on field ‘f’, are actually faint stars. Our dataset then contains approximately 66495 genuine faint galaxies.

#### 4 CALCULATING $\omega(\theta)$

The angular correlation function  $\omega(\theta)$  was calculated separately for fields ‘e’ and ‘f’. For field ‘e’ we used all galaxies brighter than a series of limits from  $R = 21.0$  to  $R = 23.5$ , and on field ‘f’ used the same faint limits but also excluded  $R < 19.0$  objects. To calculate  $\omega(\theta)$  for a field containing  $N_{gal}$  galaxies in the chosen magnitude range, we counted the separations of all  $\frac{1}{2}N_g(N_g - 1)$  possible pairs of galaxies in bins of width  $\Delta(\log \theta) = 0.2$ , giving the function  $N_{gg}(\theta_i)$ .

For each field  $N_r = 100000$  points were placed at random over the area covered by real data. i.e. avoiding any gaps or holes. The separations between the galaxies and the random points, taking the real galaxies as the centres and giving  $N_r N_g$  galaxy-random pairs in total, were similarly binned, giving  $N_{rg}(\theta_i)$ . We might then estimate  $\omega(\theta)$  for each bin as simply (Roche et al. 1993, 1996)

$$\omega(\theta_i) = \frac{N_{gg}(\theta_i)}{N_{gr}(\theta_i)} \frac{2N_r}{(N_g - 1)} - 1 \quad (5)$$

However, we found that  $\omega(\theta)$  calculated in this way showed some irregularity at large scales of  $\theta > 5$  arcmin. This was significantly improved by subtracting the random-galaxy correlation  $\omega_{rg}(\theta)$  (see e.g. Infante and Pritchett 1995). From the same sets of galaxies and random points, we counted

the  $\frac{1}{2}N_r(N_r - 1)$  random-random pairs in bins of  $\theta$ , giving  $N_{rr}(\theta)$ , and counted the  $N_r N_g$  random-galaxy pairs, this time taking the random points as the centres, giving  $N_{rg}(\theta)$ .

The random-galaxy correlation is then

$$\omega_{rg}(\theta_i) = \frac{N_{rg}(\theta_i)}{N_{rr}(\theta_i)} \frac{(N_r - 1)}{2N_g} - 1 \quad (6)$$

and the estimate of  $\omega(\theta)$  is now

$$\omega(\theta_i) = \frac{N_{gg}(\theta_i)}{N_{gr}(\theta_i)} \frac{2N_r}{(N_g - 1)} - \frac{N_{rg}(\theta_i)}{N_{rr}(\theta_i)} \frac{(N_r - 1)}{2N_g} \quad (7)$$

Figures 3 and 4 show  $\omega(\theta)$  calculated with equation (7) for fields ‘e’ and ‘f’ respectively. The error bars were derived by recalculating  $\omega(\theta)$  10 times for each field, each time excluding one of the CCD images (randomly chosen) from the analysis. In the case of field ‘e’, the error for the full field of 27 images was estimated by multiplying the scatter between these 10 runs with 26 images by  $\sqrt{26 \times \frac{26}{27}} = 5.00$ . For field ‘f’, the error for a full field of 20 images was estimated by multiplying the scatter between the 10 runs with 19 images by  $\sqrt{19 \times \frac{19}{20}} = 4.25$ .

If the real galaxy  $\omega(\theta)$  is of the form  $A\theta^{-0.8}$ , the observed  $\omega(\theta)$  will follow the form  $\omega(\theta) = A\theta^{-0.8} - C$ , with amplitude  $A$  (defined here at a one-degree separation), and a negative offset  $C$  known as the integral constraint. This offset results from the restricted area of the observation, and can be estimated by doubly integrating an assumed true  $\omega(\theta)$  over an area corresponding to each field, i.e.

$$C = \int \int \omega(\theta) d\Omega_1 d\Omega_2 \quad (8)$$

This calculation can be done numerically using the random-random correlation –

$$C = \frac{\sum N_{rr}(\theta)\theta^{-0.8}}{\sum N_{rr}(\theta)} \quad (9)$$

There is an added complication in that, at least on field ‘e’,  $\omega(\theta)$  shows an excess at  $2 < \theta < 5$  arcsec above the inwards extrapolation of the power-law at larger scales. Hence we fit two  $\theta^{-0.8}$  power-laws to  $\omega(\theta)$ , one at  $\theta > 5$  arcsec to derive an amplitude  $A$ , another at  $2 < \theta < 5$  arcsec to derive a ‘small scale amplitude’  $A_s$  (the observed  $\omega(\theta)$  at  $\theta < 2$  arcsec is ignored as it will be affected by merging of detections). For both fits, the integral constraint is  $AC_1 + A_s C_2$  where  $C_1$  is the summation of equation (9) at all angles  $\theta > 5$  arcsec and  $C_2$  the summation of equation (9) at  $2 < \theta < 5$  arcsec only. For field ‘e’,  $C_1 = 1.798$  and  $C_2 = 0.00185$  and for field ‘f’,  $C_1 = 2.022$  and  $C_2 = 0.00253$ . As the integral constraint is greatly dominated by the large-scale  $\omega(\theta)$ , so we can neglect the contribution from any small-scale excess and assume the integral constraint to be  $A(C_1 + C_2)$ . We then estimate  $A$  by least-squares fitting  $A(\theta^{-0.8} - (C_1 + C_2))$  to the observed  $\omega(\theta)$  from 5 arcsec, to a maximum separation of 7962 arcsec on field ‘e’ and 5024 arcsec on field ‘f’. Once  $A$  has been determined, giving the integral constraint,  $A_s$  is determined by fitting  $A_s \theta^{-0.8} - A(C_1 + C_2)$ , to the two bins at  $2 \leq \theta < 5$  arcsec. The fitted functions are plotted with the observed  $\omega(\theta)$  on Figures 3 and 4.

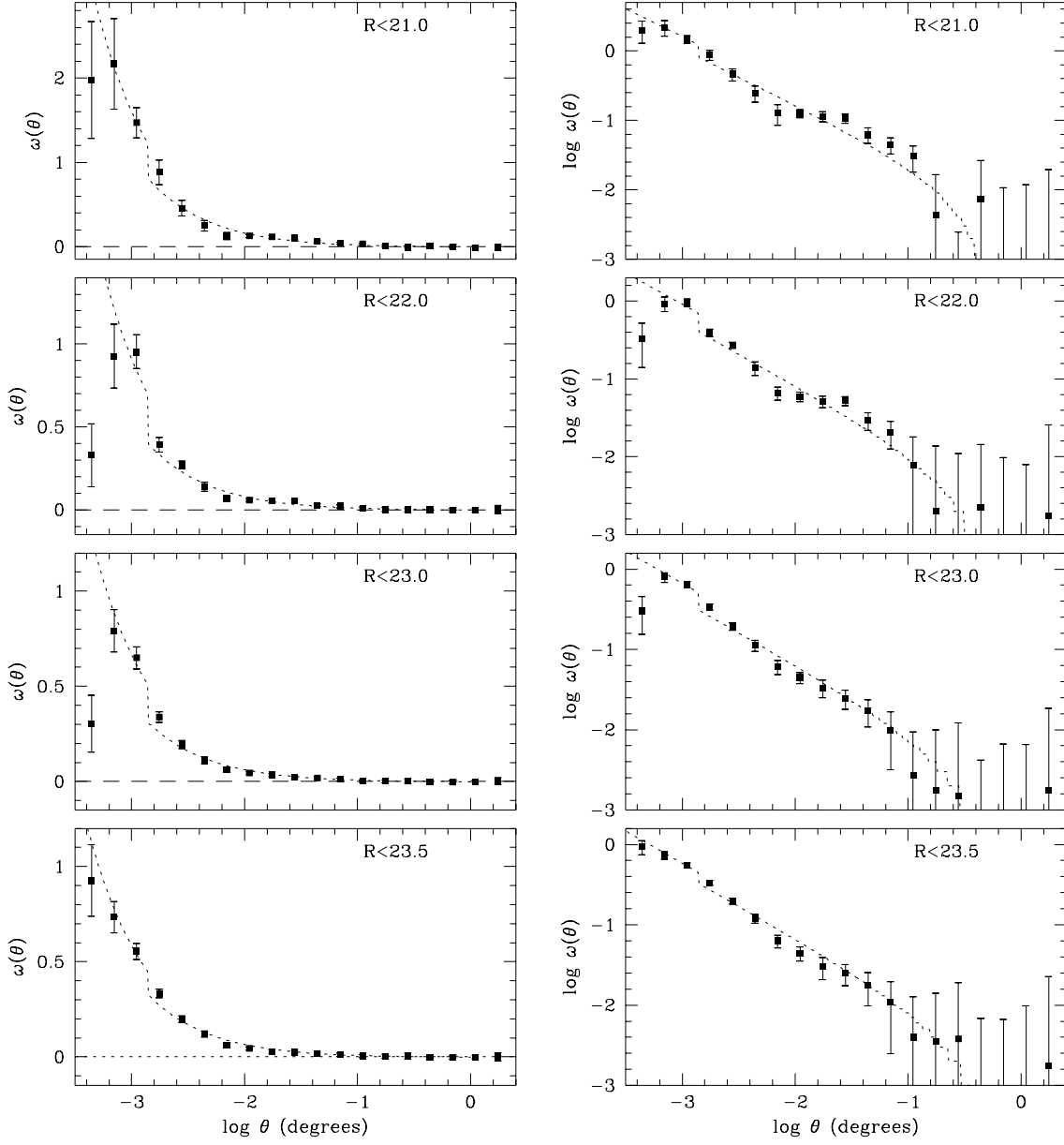
**Table 2.** Observed  $\omega(\theta)$  amplitudes at  $\theta > 5$  arcsec ( $A$ ) and at  $2 < \theta < 5$  arcsec ( $A_s$ ), in units of  $10^{-4}$  at  $1^\circ$ , and the number of galaxies ( $N_{gal}$ ), at a series of  $R$  magnitude limits

$R$ limit	$A$	$A_s$	$N_{gal}$
		Field ‘e’	
21.0	$42.44 \pm 4.67$	$64.10 \pm 8.79$	4767
21.5	$27.00 \pm 2.64$	$42.66 \pm 5.65$	7840
22.0	$20.98 \pm 1.78$	$36.36 \pm 4.37$	12608
22.5	$17.86 \pm 1.95$	$32.57 \pm 3.25$	19562
23.0	$16.27 \pm 2.10$	$26.59 \pm 2.47$	29444
23.5	$17.18 \pm 1.96$	$23.38 \pm 1.87$	42971
		Field ‘f’	
21.0	$23.50 \pm 2.89$	$24.90 \pm 6.89$	4852
21.5	$14.46 \pm 2.63$	$14.07 \pm 4.32$	8461
22.0	$11.62 \pm 1.85$	$9.13 \pm 3.60$	13114
22.5	$11.30 \pm 2.27$	$11.19 \pm 3.60$	18861
23.0	$11.69 \pm 2.48$	$11.63 \pm 3.93$	26334
23.5	$13.24 \pm 2.75$	$14.49 \pm 3.62$	35321

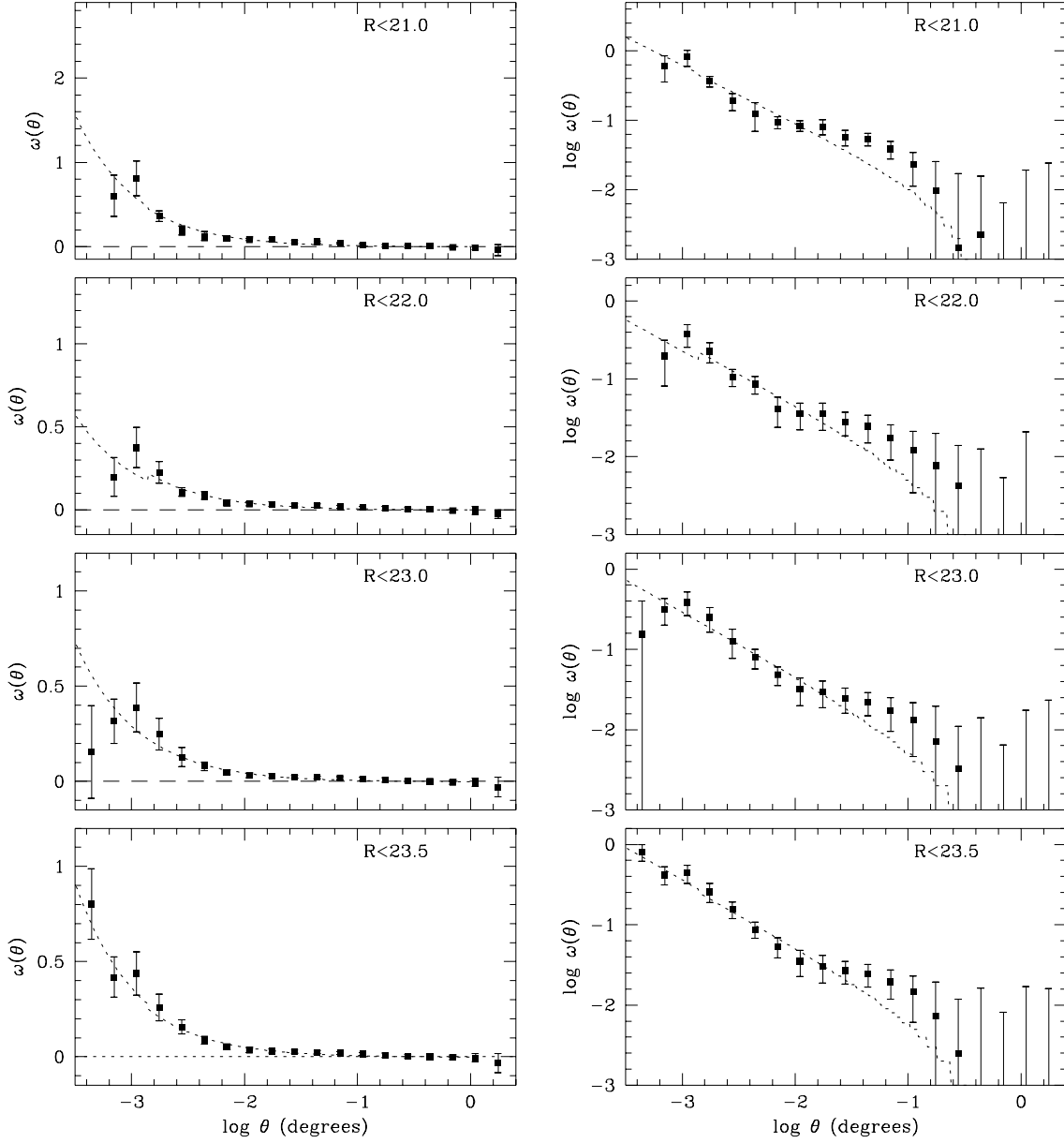
## 5 $\omega(\theta)$ RESULTS

Table 2 gives the fitted  $A$  and  $A_s$  amplitudes at magnitude limits of  $R = 21.0$  to  $R = 23.5$ . The errors were estimated by fitting amplitudes to our measurements of  $\omega(\theta)$  from datasets with one image excluded, and multiplying the scatter between these amplitudes by 5.00 for field ‘e’ and by 4.25 for field ‘f’.

However, the fitted amplitudes will be underestimates due to the effects of star contamination. A fraction of (randomly distributed) stars  $f_s$  within the galaxy sample will reduce the observed  $\omega(\theta)$  at all angles by a factor of  $(1 - f_s)^{-2}$ . As described in Section 3, we estimate the fraction of faint ( $R > 20.5$ ) stars  $f_s$  in the sample of objects classed as galaxies, for each field at each magnitude limit. Table 3 gives our estimates of  $f_s$ , together with amplitudes  $A$  and  $A_s$  corrected for star contamination by multiplying by  $(1 - f_s)^{-2}$ .



**Figure 3.** Observed  $\omega(\theta)$  for galaxies on field ‘e’ brighter than  $R = 21.0, 22.0, 23.0$  and  $23.5$ , as log-linear (left) and log-log (right) plots. The dotted lines show the best-fit two-part  $\theta^{-0.8}$  power-laws with the integral constraint offset.



**Figure 4.** Observed  $\omega(\theta)$  for galaxies on field ‘f’ fainter than  $R = 19.0$  and brighter than  $R = 21.0, 22.0, 23.0$  and  $23.5$ , as log-linear (left) and log-log (right) plots. The dotted lines show the best-fit two-part  $\theta^{-0.8}$  power-laws with the integral constraint offset.



**Table 3.** Estimated fraction of stars  $f_s$  contaminating the galaxy samples at each magnitude limit, and the  $\omega(\theta)$  amplitudes at  $\theta > 5$  arcsec ( $A$ ) and  $2 < \theta < 5$  arcsec ( $A_s$ ) multiplied by a correction for star contamination,  $(1 - f_s)^{-2}$ .

$R$ limit	$f_s$	$A$ (corrected)	$A_s$ (corrected)
Field ‘e’			
21.0	0.0313	$45.23 \pm 4.97$	$68.31 \pm 9.37$
21.5	0.0948	$32.95 \pm 3.22$	$52.06 \pm 6.89$
22.0	0.1167	$26.89 \pm 2.29$	$46.60 \pm 5.61$
22.5	0.1144	$22.78 \pm 2.48$	$41.53 \pm 4.46$
23.0	0.1037	$20.25 \pm 2.62$	$33.10 \pm 3.07$
23.5	0.0910	$20.80 \pm 2.37$	$28.29 \pm 2.26$
Field ‘f’			
21.0	0.1607	$33.36 \pm 4.10$	$35.34 \pm 9.77$
21.5	0.2403	$25.05 \pm 4.55$	$24.38 \pm 7.49$
22.0	0.2594	$21.19 \pm 3.38$	$16.64 \pm 6.57$
22.5	0.2571	$20.47 \pm 4.11$	$20.27 \pm 6.53$
23.0	0.2421	$20.35 \pm 4.31$	$20.25 \pm 6.84$
23.5	0.2260	$22.09 \pm 4.59$	$24.18 \pm 6.04$

These results show that, firstly, our detection of clustering at  $R \leq 23.5$  is of high significance, an estimated  $8.75\sigma$  on field ‘e’ and  $4.81\sigma$  on field ‘f’, or  $10\sigma$  overall. Secondly, although the measured  $\omega(\theta)$  amplitudes at  $\theta > 5$  arcsec are lower for field ‘f’ than for field ‘e’, they become reasonably consistent when the greater star contamination on field ‘f’ is taken into account. Thirdly, on field ‘e’ the  $\omega(\theta)$  amplitude is significantly higher at  $2 < \theta < 5$  arcsec than at larger separations, by  $3.7\sigma$  at  $R \leq 22.5$ , whereas on field ‘f’ we find no significant difference between  $A$  and  $A_s$ . We leave the interpretation of  $A_s$  to Section 7 and first discuss the results at  $\theta > 5$  arcsec.

Infante and Pritchett (1995) claimed that the slope of  $\omega(\theta)$  in their photographic survey flattened on going faintward, from  $\delta = 0.94 \pm 0.04$  at  $F < 21$  to  $\delta = 0.65 \pm 0.05$  at  $F < 23$ , and attributed this to a flatter  $\xi(r)$  for later Hubble types. However, Couch et al. (1993) found no significant change in  $\delta$  over this magnitude range. We estimate a best-fit  $\delta$  by least-squares fitting ‘ $A(\theta^{-\delta} - C)$ ’ to  $\omega(\theta)$  at  $\theta > 5$  arcsec, for a series of slopes  $\delta$ , each time recalculating the integral constraint as

$$C = \frac{\sum N_{rr}(\theta)\theta^{-\delta}}{\sum N_{rr}(\theta)}. \quad (10)$$

Table 4 gives the values of  $\delta$  which minimize the  $\chi^2$  of the fits. For field ‘e’ a slope was also fitted to  $\omega(\theta)$  at  $\theta > 8$  arcsec only, where the excess of small scale clustering will have less effect on  $\delta$ . Errors on  $\delta$  were estimated by the same method as the errors on the amplitude, i.e. fitting the same functions to  $\omega(\theta)$  calculated from datasets with one image excluded.

In contrast to Infante and Pritchett (1995), we find no flattening of  $\delta$  over this magnitude range. On field ‘e’ the power-law fits suggest if anything a slight steepening on going faintward, but this is not really statistically significant, and might simply be due to the effect of the close pair excess extending to slightly larger scales. The assumption of a constant  $\delta = 0.8$  slope in fitting an amplitude appears a reasonable approximation for this data.

Figure 5 shows the scaling of the  $\omega(\theta)$  amplitude with  $R$  magnitude limit, for this data and several other  $R$ -band

**Table 4.** Best-fitting power-laws ( $\delta$ ) for  $\omega(\theta)$ 

$R$ limit	Field ‘e’ $\theta > 5$ arcsec	Field ‘e’ $\theta > 8$ arcsec	Field ‘f’ $\theta > 5$ arcsec
21.0	$0.90 \pm 0.08$	$0.87 \pm 0.08$	$0.75 \pm 0.10$
21.5	$0.86 \pm 0.08$	$0.77 \pm 0.08$	$0.85 \pm 0.18$
22.0	$0.92 \pm 0.08$	$0.89 \pm 0.09$	$0.78 \pm 0.18$
22.5	$0.96 \pm 0.07$	$0.91 \pm 0.09$	$0.79 \pm 0.18$
23.0	$1.06 \pm 0.09$	$1.01 \pm 0.09$	$0.81 \pm 0.27$
23.5	$1.08 \pm 0.10$	$1.04 \pm 0.11$	$0.83 \pm 0.18$

surveys, plotted as the amplitude at one degree when a  $\theta^{-0.8}$  power-law is fitted. The magnitude limits of other surveys were converted into approximate equivalents in our  $R$  band. For the four red-band CCD surveys, we assume  $R = R(\text{Roche et al. 1993}) - 0.02$ ,  $R = R(\text{Roche et al. 1996}) + 0.02$ ,  $R = R(\text{Woods and Fahlman})$  and  $R = r(\text{Brainerd et al.}) - 0.55$ , and for the Infante and Pritchett (1995)  $F$ -band photographic survey we assume  $R = F - 0.14$  from the correction listed by Metcalfe et al. (1991). Couch et al. (1993) used a broad ‘VR’ passband, and Villumsen et al. (1997) give  $\omega(\theta)$  amplitudes from the Hubble Deep Field as a function of  $V_{606}$  limit. For these bluer passbands, we assume  $R = VR - 0.35$  and  $R = V_{606} - 0.39$ , as derived from the spectrum of an evolving Sbc galaxy model (Section 6.1) at  $z \sim 0.5$ .

There is considerable scatter between the observations, with our  $\omega(\theta)$  amplitudes lying towards the upper end of the observed range. At  $R \leq 23.5$ , our  $\omega(\theta)$  amplitude appears to exceed that of Roche et al. (1993) by a factor of  $\sim 2$  and  $\sim 3\sigma$ , but the earlier result was not corrected for star-contamination and was derived from much smaller fields. Our new  $\omega(\theta)$  amplitudes agree with the relatively high normalization of the Infante and Pritchett (1995) and the Woods and Fahlman (1997)  $\omega(\theta)$  scaling.

The results from this data alone might give some suggestion of a levelling-out of the  $\omega(\theta)$  scaling at  $R \sim 22.5$ – $23.5$ , but a comparison with Brainerd et al. (1995) and Villumsen et al. (1997) (and also the  $B < 27$  results of Metcalfe et al. 1995) indicates that the  $\omega(\theta)$  amplitude does continue to decrease at  $R > 23.5$ , falling by as much as a further order of magnitude at  $R \sim 26$ – $29$ .

The interpretation of these results is discussed further in Sections 6.3 and 9.

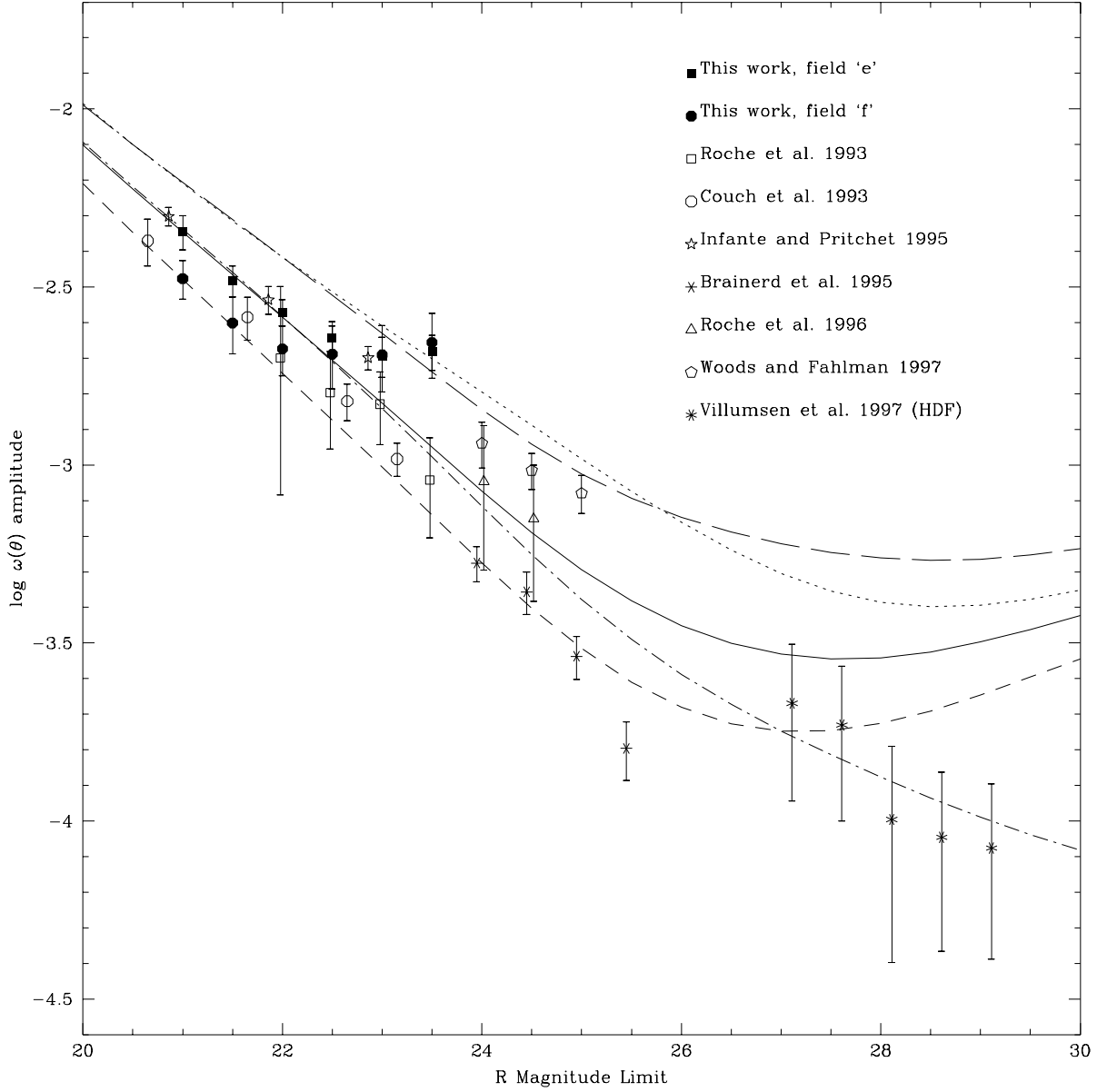


**Figure 5.** The  $\omega(\theta)$  amplitude at  $\theta > 5$  arcsec for the galaxies in our two fields, against  $R$  magnitude limit, compared with  $\omega(\theta)$  amplitudes from other faint galaxy surveys and five models described in Section 6; model A, non-evolving,  $\epsilon = 0$  (dotted); model B, PLE,  $\epsilon = 0$  (solid); model C, PLE,  $\epsilon = 1.2$  clustering evolution (short-dashed); model D, PLE  $\epsilon = -1.2$  comoving clustering (long-dashed); model E, PLE,  $\epsilon = 0$ , with a  $L^{-0.25}$  decrease in the strength of clustering with luminosity (dot-dash).

## 6 MODELS OF $\omega(\theta)$

### 6.1 Modelling of Galaxy Evolution

In order to interpret the faint galaxy  $\omega(\theta)$ , we need a model which generates a redshift distribution  $N(z)$  for each type of galaxy, which is as consistent as possible with observations. In this paper the results are compared with a Pure Luminosity Evolution (PLE) model, i.e. a model in which the characteristic luminosity of the galaxy luminosity function,  $L^*$ , evolves with redshift but the normalization  $\phi^*$  and slope  $\alpha$  are assumed constant. The model used here is an updated version of the ‘size and luminosity evolution’ model of Roche et al. (1998a), in which elliptical galaxies form in a short starburst at high redshift but spirals form by a more gradual inside-outwards process. The model was updated by (i) assuming similar star-formation histories to the previous version with the new ‘bc96’ stellar evolutionary models (e.g. Charlot, Worthey and Bressan 1996), with a Salpeter IMF, solar metallicity for E/S0/Sab/Sbc galaxies and 0.4 solar metallicity for Scd/Sdm and Starburst galaxies (ii) improving the modelling of dust extinction – the optical depth of dust is now

$$\tau_{dust}(\lambda) = \beta_{dust} \times \frac{10^{10}}{M_{gal}} \frac{dM}{dt} \tau_M(\lambda) \quad (11)$$

where  $\frac{dM}{dt}$  is the SFR in  $M_\odot \text{ yr}^{-1}$ ,  $M_{gal}$  the total galaxy mass (stars and gas), and  $\tau_M(\lambda)$  the tabulated ‘Rv=3.1’ Galactic dust extinction law of Mathis (1990), normalized to unity at 4500Å, and  $\beta_{dust} = 1.0$  for E/S0 galaxies, 0.4 for Sab spirals 0.3 for Sbc spirals and 0.12 for Scd/Sdm/Starburst galaxies.

For the purposes of this paper, the important features of this model are that (i) both elliptical and spiral galaxies undergo an evolutionary brightening out to  $z \sim 1-2$ , (ii) the faint-end slope of the galaxy luminosity function depends strongly on Hubble type, steepening from  $\alpha = -0.7$  for E/S0 galaxies to  $\alpha = -1.5$  for Scd galaxies and the Marzke et al. (1994) luminosity function, with  $\alpha = -1.87$  but a low  $\phi^*$ , for Sdm and starburst galaxies.

For comparison, we also consider a non-evolving model, with the same  $z = 0$  luminosity functions as the PLE model, and k-corrections derived by redshifting without evolution the galaxy spectra given by the PLE models at  $z = 0$ .

Figure 1 shows how the  $L^*$  evolution in the PLE model increases the predicted galaxy number counts, and gives a good fit to the observed counts. Figure 6 shows the galaxy redshift distributions  $N(z)$  predicted by both models at  $R = 21-23.5$  limits. At  $z < 1.2$  the PLE model agrees well with the  $N(z)$  in Roche et al. (1998a). In the PLE model, a ‘tail’ of  $1 < z < 2$  galaxies appears between  $R = 22$  and  $R = 23$ , whereas with no  $L^*$  evolution very few  $z > 1$  galaxies would be seen even at the survey limit of  $R = 23.5$ . Deep spectroscopy (Cowie et al. 1996) reveals that  $1 < z < 1.8$  galaxies do start to appear in substantial numbers at  $B > 23.2$  ( $R \gtrsim 22.7$ ), in general agreement with this PLE model. The PLE model is also reasonably consistent with the numbers and surface brightness of the  $z > 2.5$  ‘Lyman break’ galaxies on the Hubble Deep Field, although these more distant galaxies are not expected to be visible within this survey.

Figure 7a shows the mean redshift of both models as a function of  $R$  magnitude limit. At the survey limit of  $R =$

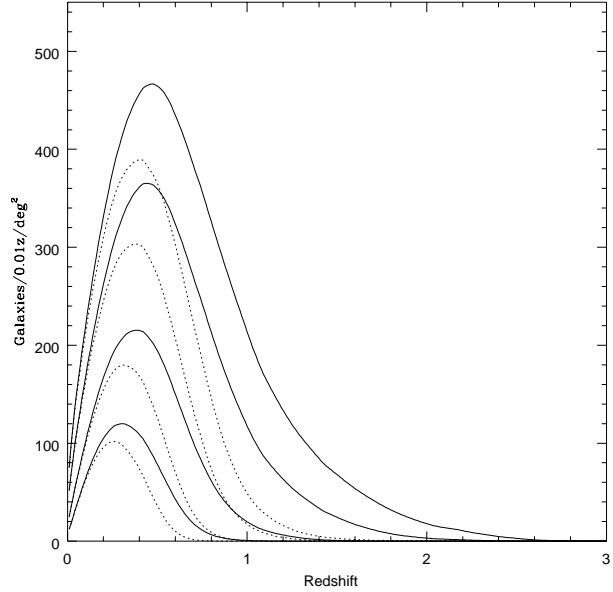


**Figure 6.** Galaxy redshift distributions predicted for all galaxies to limits of (from lowest to highest),  $R = 21.0, 22.0, 23.0$  and  $23.5$ , for the PLE (solid) and no-evolution (dotted) models.

$23.5$ , the PLE model predicts  $z_{mean} = 0.69$ , which increases on going further faintward until  $R \sim 27$ , where galaxies will be seen at all redshifts to the epoch of formation and  $z_{mean}$  levels out at  $z \sim 1.5$ .

As we seem to have a model which reproduces the galaxy counts and  $N(z)$  reasonably well, we can now put it to use in interpreting the  $\omega(\theta)$  amplitudes.

### 6.2 From $N(z)$ to $\omega(\theta)$

The  $\omega(\theta)$  amplitude is predicted using the Limber’s formula integration of  $\xi(r, z)$  over the modelled  $N(z)$ . We assume the form given in the Introduction,

$$\xi(r, z) = (r/r_0)^{-\gamma} (1+z)^{-(3+\epsilon)} \quad (12)$$

where  $r_0$  normalizes the strength of clustering at  $z = 0$ ,  $\gamma$  is the slope and  $\epsilon$  parameterizes the clustering evolution relative to the  $\epsilon = 0$  stable clustering model.

The  $\omega(\theta)$  amplitude will generally decrease on going faintward, primarily as a result of  $N(z)$  becoming more extended, but there may be additional effects due to the evolution of clustering and to changes in the proportions of different types of galaxy. The model of Roche et al. (1996) assumed  $\gamma = 1.8$  for all galaxy types, with the  $r_0$  as derived by Loveday et al. (1985, hereafter LMEP) from the cross-correlation of the Stromlo-APM redshift survey with the APM catalog –  $r_0 = 5.9 h^{-1} \text{ Mpc}$  for E/S0 galaxies and  $r_0 = 4.4 h^{-1} \text{ Mpc}$  for later types, and also assumed that dwarf galaxies (those with  $z = 0$  blue-band absolute magnitudes  $M_B > -20.5$ ) are half as clustered as those of higher luminosity, again from LMEP.

With stable clustering and  $L^*$  evolution, this model predicted a  $\omega(\theta)$  scaling fairly consistent with the observations in the blue-band (Roche et al. 1996), but it underpredicted the  $\omega(\theta)$  amplitudes from  $K$ -band surveys at  $K \simeq 19.5-21.5$

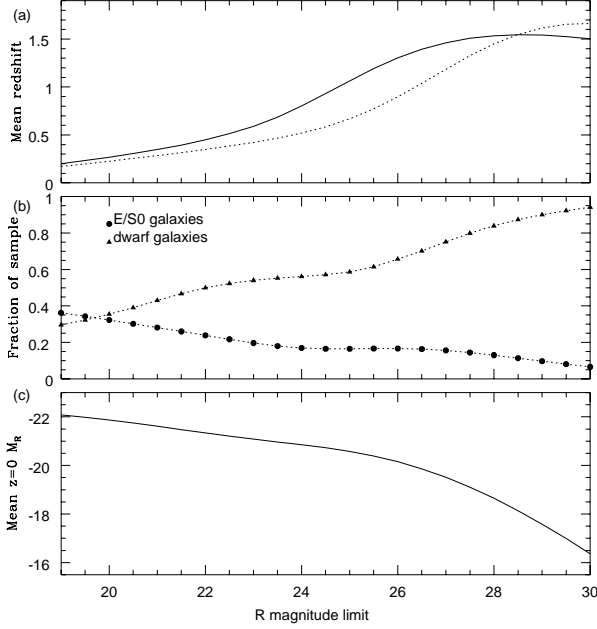


**Figure 7.** (a) Mean redshift as a function of  $R$  magnitude limit for PLE (solid) and non-evolving (dotted) models. (b) The fractions of E/S0 galaxies and dwarf galaxies (those with  $M_B > -20.5$  at  $z = 0$ ) as a function of  $R$  magnitude limit for the PLE model. (c) The mean  $M_R$  at  $z = 0$  as a function of magnitude limit in the PLE model.

limits (Roche et al. 1998b; Carlberg et al. 1997), in which E/S0 galaxies will be more prominent. The  $K$ -band results were fitted better by adopting the Guzzo et al. (1997)  $\xi(r)$  for giant ( $M_B \lesssim -21.5$ ) E/S0 galaxies, with stronger clustering of  $r_0 = 8.35 \pm 0.75 h^{-1}$  Mpc and  $\gamma = 2.05 \pm 0.09$ .

The  $r_0$  used by Roche et al. (1996) were derived by LMEP from a cross-correlation of each type of galaxy with all APM galaxies, a method which would tend to underestimate the differences between the  $\xi(r)$  of the galaxy types. LMEP also derive  $\xi(r)$  using a different ‘inversion’ method, which gave  $r_0 = 7.76 \pm 0.15 h^{-1}$  Mpc and  $\gamma = 1.87 \pm 0.07$  for early-types (of all luminosities) and  $r_0 = 4.49 \pm 0.13 h^{-1}$  Mpc and  $\gamma = 1.72 \pm 0.05$  for early-types. These estimates would be more consistent with Guzzo et al. (1997) and the results from the  $K$ -band. In this paper we model  $\xi(r)$  with, for simplicity, a single slope  $\gamma = 1.8$ , and take the normalization from the LMEP ‘inversion’ estimates at  $r = 1 h^{-1}$  Mpc. This gives for early-types  $(r_0)^{1.8} = 7.76^{1.87}$  and thus  $r_0 = 8.4 h^{-1}$  Mpc, and for late-types  $(r_0)^{1.8} = 4.49^{1.72}$  giving  $r_0 = 4.2 h^{-1}$  Mpc.

In the Limber’s formula integration, we apply a weighting term to the galaxy clustering at each redshift derived from the predicted fraction of ellipticals ( $f_e$ ). With our assumed  $r_0$ ,  $\xi_{\text{elliptical}} \simeq 3.5\xi_{\text{spiral}}$ , and the cross-correlation between early and late type is assumed to be the geometric mean of their autocorrelations so that  $\xi_{\text{cross}} \simeq 1.87\xi_{\text{spiral}}$ . We therefore normalize our models to the LMEP spiral galaxy  $r_0$  and apply an additional weighting factor of  $(1 - f_e)^2 + 3.5f_e^2 + 2 \times 1.87f_e(1 - f_e)$  to the clustering at each redshift.

The luminosity dependence of clustering is modelled by two methods, the first the same as in Roche et al. (1996). Ac-

cording to LMEP, lower luminosity ( $M_B > -20.5$ ) galaxies are less clustered than more luminous galaxies of the same Hubble type by a factor of 2 at  $r \sim 1 h^{-1}$  Mpc. At each redshift, the models calculate  $f_d$ , the fraction of galaxies which would have  $M_B > -20.5$  at  $z = 0$ , and apply a luminosity weighting, normalized to be unity for the dwarf fraction in the LMEP dataset, of  $1.2(1 - f_d)^2 + 0.6f_d^2 + 2 \times 0.85(1 - f_d)f_d$ .

Figure 7b shows the PLE model prediction for  $f_e$  and  $f_d$  as a function of  $R$  limit –  $f_e$  slowly decreases (from 0.28 to 0.18 between  $R \leq 21$  and  $R \leq 23.5$ ) while  $f_d$  increases. Both these trends would slightly steepen the  $\omega(\theta)$  scaling. Dwarf galaxies (almost all of late type, at least in the field environment) will dominate the sample at  $R \gtrsim 26$ , as  $L^*$  galaxies are seen to their highest redshifts at these magnitudes and on going fainter we simply look down the faint-end of the galaxy luminosity function for the same volume of space.

Using the luminosity evolution and  $r_0$  described above, we predict the scaling of  $\omega(\theta)$  with  $R$  magnitude limit for four models

A:  $N(z)$  from non-evolving model,  $\epsilon = 0$

B:  $N(z)$  from PLE model,  $\epsilon = 0$

C:  $N(z)$  from PLE model, clustering evolution of  $\epsilon = 1.2$ .

D:  $N(z)$  from PLE model, comoving clustering of  $\epsilon = -1.2$ .

We also plot a fifth model E, which differs from model B only in the luminosity dependence of  $\xi(r)$ . Here the strength of clustering varies continuously with the unevolved luminosity (i.e. very approximately the mass) of the galaxies, as  $\xi(r) \propto L^{0.25}$ . The luminosity weighting term in Limber’s formula is then  $10^{-0.1(\langle M_R \rangle + 22.0)}$ , where  $\langle M_R \rangle$  is the mean unevolved (i.e. at  $z = 0$ )  $R$ -band absolute magnitude of all galaxies at a given redshift, and the addition of 22.0 normalizes the model to the same  $\omega(\theta)$  amplitude as model B at  $R \sim 22.0$ . Model E would be approximately consistent with the LMEP results, in which galaxy subsamples differing by 2.2 mag in mean absolute magnitude differed by a factor of 2 in  $\xi(r)$ , and with the Guzzo et al. (1997) dependence of  $r_0$  on magnitude limit, but the model includes the additional assumption that clustering continues to decrease at lower luminosities, becoming very weak for the faintest dwarfs. Figure 7c shows how the mean unevolved luminosity decreases slowly to  $R \sim 25.5$ , then more rapidly as the sample becomes dwarf-dominated – consequently the differences between model E and the others is most apparent at  $R \gtrsim 25.5$ .

### 6.3 Comparison with Observations

Figure 5 shows the five models against the  $\omega(\theta)$  observations. Model A gives  $\omega(\theta)$  amplitudes well above most of the data and can be rejected (redshift surveys have already excluded models with no  $L^*$  evolution). To  $R \sim 25$ , PLE model B passes through the middle of the rather scattered data points. Our results agree well with this model except for showing some excess in the faintest point. However, model B predicts a levelling out of the  $\omega(\theta)$  scaling at  $R > 26$ , as  $N(z)$  reaches its maximum extension, whereas the data suggest a continuing decrease. In particular, model B appears to overpredict the very weak clustering of the faintest Hubble Deep Field galaxies.

Model C, with clustering evolution of  $\epsilon = 1.2$ , passes through the lowest of the data points at  $R < 25$ . It is a little more consistent with the  $R > 25$  amplitudes than model

B, although it predicts a slight rise in  $\omega(\theta)$  amplitude at  $R > 27$  (where  $z_{mean}$  no longer increases), while Villumsen et al. (1997) find a marginal decrease. At  $R = 21\text{--}23.5$ ,  $\epsilon = 1.2$  clustering evolution reduces  $\omega(\theta)$  0.134–0.191 dex below the model B prediction. It underpredicts our results by approximately the same factor, and as our statistical errors are only  $\sim 10\%$ , can be rejected by at least  $\sim 3\sigma$ . The comoving model D gives a very similar  $\omega(\theta)$  scaling to the non-evolving model A, overpredicting the faint galaxy clustering, and can be rejected. If we assume the  $N(z)$  and  $r_0$  in our PLE model to be correct and treat  $\epsilon$  as a free parameter, a comparison of the model at  $R = 21\text{--}23.5$  with our field ‘e’ and field ‘f’ results combined give a minimum  $\chi^2$  for  $\epsilon = -0.03 \pm 0.44$ . Stable clustering is clearly favoured with a  $2\sigma$  upper limit of  $\epsilon = 0.85$  on the rate of clustering evolution.

To  $R \sim 24$ , the  $\omega(\theta)$  scaling from model E does not differ significantly from model B, so it is similarly consistent with our results. It differs from models A–D at  $R > 25.5$ , where the decrease in  $r_0$  with luminosity causes the  $\omega(\theta)$  amplitude to continue falling after  $z_{mean}$  has reached its maximum. This results in a much better fit to the Hubble Deep Field clustering than the other 4 models.

## 7 THE SMALL-SCALE $\omega(\theta)$ AND MERGER RATE EVOLUTION

For a sample of  $R < 21.5$  galaxies, Infante et al. (1996) found that the  $\omega(\theta)$  at  $\theta < 6$  arcsec was still a  $\delta \simeq 0.8$  power-law but with an amplitude about a factor 1.8 higher than at  $\theta > 6$  arcsec. We investigated whether this was the case in our data (Section 4) by fitting a  $\omega(\theta)$  amplitude  $A$  at  $\theta > 5$  arcsec and a second ‘small scale amplitude’  $A_s$  at  $2 < \theta < 5$  arcsec. On field ‘e’,  $A_s > A$  at all magnitude limits, but on field ‘f’ there was no significant difference between  $A$  and  $A_s$ . The reason for the discrepancy is not clear but it may be related to the poorer seeing on some ‘f’ images and the less uniform sky background and greater star contamination on all the ‘f’ data. Previous studies of the numbers of close pairs of faint galaxies show great variations between datasets, suggesting a critical dependence on the resolution and quality of the data (Roche et al. 1998b). The  $\omega(\theta)$  from the ‘f’ field (Figure 3) shows a drop at  $\theta < 3.2$  arcsec only seen in the ‘e’ field at  $\theta < 2$  arcsec, suggesting that poor resolution is the cause. Hence for the remainder of this Section, we consider only the  $A_s$  from field ‘e’, and bear in mind that even these may be an underestimate.

At the mean redshift of the Infante et al. (1996) sample,  $z_{mean} \simeq 0.35$ ,  $\theta \leq 6$  arcsec corresponds to a projected physical separation  $\lesssim 20 h^{-1}$  kpc. Even locally, there is an excess of  $\lesssim 20 h^{-1}$  kpc pairs above the number expected from normal galaxy clustering. This is made up of strongly interacting galaxies or those spiralling together in the early stages of merging. In the  $B < 14.5$ ,  $z_{mean} = 0.007$  UGC catalog, some  $4.6 \pm 0.4\%$  of all galaxies are in physical pairs of projected separation  $< 19 h^{-1}$  kpc (Carlberg et al. 1994).

We interpret our results by deriving a similar ‘close pair fraction’,  $f_{pairs}$ , here defined as the fraction of the galaxies which are in  $\theta < 5$  arcsec pairs above that which would be expected from chance and from the projection of the clustering measured at  $\theta > 5$  arcsec. Firstly, we assume

**Table 5.** Percentage of galaxies in excess  $\theta < 5$  arcsec pairs on field ‘e’

$R$ limit	$f_{pairs}$ (percentage)
21.0	$4.03 \pm 1.85$
21.5	$5.14 \pm 2.08$
22.0	$8.32 \pm 2.60$
22.5	$12.33 \pm 3.36$
23.0	$12.88 \pm 4.05$
23.5	$11.12 \pm 4.86$

$\omega(\theta) \propto \theta^{-0.8}$  at all  $\theta < 5$  arcsec separations, so that the number of  $\theta < 2$  arcsec pairs can be estimated by an inwards extrapolation of this power-law from its  $2 < \theta < 5$  arcsec amplitude. In an unbounded area, with a surface density of galaxies  $\rho_{gal}$ , the number of  $\theta < \beta$  pairs per galaxy above the random expectation will be

$$\frac{N_{pairs}}{N_{gal}} = \rho_{gal} A \int_0^\beta 2\pi\theta\theta^{-0.8} d\theta \quad (13)$$

where  $A$  is the  $\omega(\theta)$  amplitude. To find the number of pairs above that expected from the clustering seen at larger scales, we replace  $A$  by the difference in clustering amplitudes  $A_s - A$ , so that

$$\frac{N_{pairs}}{N_{gal}} = \rho_{gal} (A_s - A) \int_0^\beta 2\pi\theta\theta^{-0.8} d\theta \quad (14)$$

which for  $\beta = 5$  arcsec gives

$$\frac{N_{pairs}}{N_{gal}} = 0.00196 \rho_{gal} (A_s - A) \quad (15)$$

In a finite field  $N_{pairs}$  will be reduced as some galaxies will lie less than 5 arcsec from the field edges or the holed areas, but this effect is minor for the large area of field ‘e’. A numerical integration over the field ‘e’ area gives

$$\frac{N_{pairs}}{N_{gal}} = 0.001938 \rho_{gal} (A_s - A) \quad (16)$$

As a pair contains two galaxies,  $f_{pair} = 2 \frac{N_{pairs}}{N_{gal}}$ . We estimate  $f_{pairs}$  at each magnitude limit using the field ‘e’  $A$  and  $A_s$  corrected for star contamination (Table 3), and also apply a correction for star contamination to the observed density of classified galaxies  $\rho_{gal}$ . Hence

$$f_{pairs} = 0.003876(1 - f_{star})\rho_{gal}(A_s - A) \quad (17)$$

which is given in Table 5, with errors from adding the errors on  $A$  and  $A_s$  in quadrature.

The excess of close pairs above the  $\omega(\theta)$  measured at larger scales is  $3.7\sigma$  significance at  $R \leq 22.5$  and  $> 3\sigma$  at  $R \leq 22$  and  $R \leq 23$ . We compare these results with Infante et al (1996), who found 1317 pairs with  $2 < \theta < 6$  arcsec pairs in a sample of 16749 galaxies with  $R < 21.5$ , compared to 477 expected by chance or 842 expected from the clustering at larger scales. The proportion of galaxies in  $2 < \theta < 6$  pairs above the large-scale  $\omega(\theta)$  is then  $2 \times \frac{1317-842}{16749} = 5.67\%$ . For a  $\theta^{-0.8}$  power-law the number of  $\theta < 5$  arcsec pairs will be 1.097 times the number at  $2 < \theta < 6$  arcsec, and the significance of the pairs excess is given as  $\sim 5\sigma$ , so the Infante et al. (1996) result corresponds to  $f_{pair} = 6.22 \pm 1.24\%$ , in good agreement with our field ‘e’ estimate at this limit.

As the timescale between the approach of two galaxies within  $\sim 20 h^{-1}$  kpc and their subsequent merging or separation,  $\sim 0.75$  Gyr (e.g. Mihos and Hernquist 1996), is short compared to the Hubble time, the merger/interaction rate  $R_m \propto f_{pair}$  approximately. The merger rate evolution is modelled as  $R_m \propto R_{m0}(1+z)^m$  and normalized using the Carlberg et al. (1994) estimate of 4.6% for the fraction of local galaxies in pairs of projected separation  $< 19 h^{-1}$  kpc. All such pairs will have an angular separation  $\theta < 5$  arcsec when the angular diameter distance  $d_A > 784 h^{-1}$  Mpc, or at  $z > 0.455$  in our chosen cosmology. At lower redshifts, if we again assume  $\omega(\theta) \propto \theta^{-0.8}$  for the close-pair galaxies, the fraction with  $\theta < 5$  arcsec will be  $(\frac{d_A(z)}{784 h^{-1}})^{1.2}$ .

For each magnitude limit we then model  $f_{pair}$  by summing

$$f_{pair} = f_{pair}(z < 0.455) + f_{pair}(z > 0.455) \quad (18)$$

where

$$f_{pair}(z < 0.455) = 0.046 \frac{\int_0^{0.455} (\frac{d_A(z)}{784 h^{-1}})^{1.2} N(z)(1+z)^m dz}{\int_0^{0.455} N(z) dz}$$

$$f_{pair}(z > 0.455) = 0.046 \frac{\int_{0.455}^6 N(z)(1+z)^m dz}{\int_{0.455}^6 N(z) dz}$$

over the PLE model  $N(z)$ .

Infante et al. (1996) estimated  $m = 2.2 \pm 0.5$  from the increase in the fraction of galaxies in close pairs from  $z = 0$  to  $z_{mean} = 0.35$ . Our data suggest that the upward trend in  $f_{pair}$  continues to fainter magnitudes, with the slight drop from  $R = 23$  to  $R = 23.5$  probably being due to less effective splitting of close pairs on approaching the limits of the data ( $f_{pair}$  decreases steeply beyond the  $R = 23.5$  limit).

Figure 8 shows  $f_{pair}$  from our field ‘e’ and from Infante et al. (1996), compared with the model (equation 18) for  $m = 0, 1, 2, 3$  and 4. The  $m = 2$  model is clearly the most consistent with the data, whereas both a non-evolving merging rate ( $m = 0$ ) and very rapid evolution of  $m > 3$  appear to be rejected. A  $\chi^2$  test of the model against the plotted data (excluding the  $R = 23.5$  point) gives a best-fitting merger rate evolution of  $m = 1.65^{+0.62}_{-0.88}$ . Evolution of  $m > 3.12$  is rejected at the  $\geq 3\sigma$  level. This is discussed further in Section 9.2.

## 8 HIGHER-ORDER CORRELATIONS

The large size of our galaxy sample may enable us to investigate the higher order correlation functions, which may discriminate between models of galaxy clustering more effectively than  $\omega(\theta)$  alone. Higher order correlations have previously been studied to  $B = 20$  in the APM survey (Gaztañaga 1994) and the Edinburgh-Durham Southern Galaxy Catalog Survey (EDSGCS) (Szapudi, Meiksin and Nichol 1996), both containing several  $\times 10^5$  galaxies.

Before discussing these results further, we define the hierarchical moments and describe their estimation from a simple counts-in-cells method.

Consider a survey area divided into  $m$  cells of area  $\Omega$ , with  $N_i$  galaxies in cell  $i$  and a mean number of galaxies per cell  $\bar{N}$ . The moments of the distribution of counts-in-cells will be

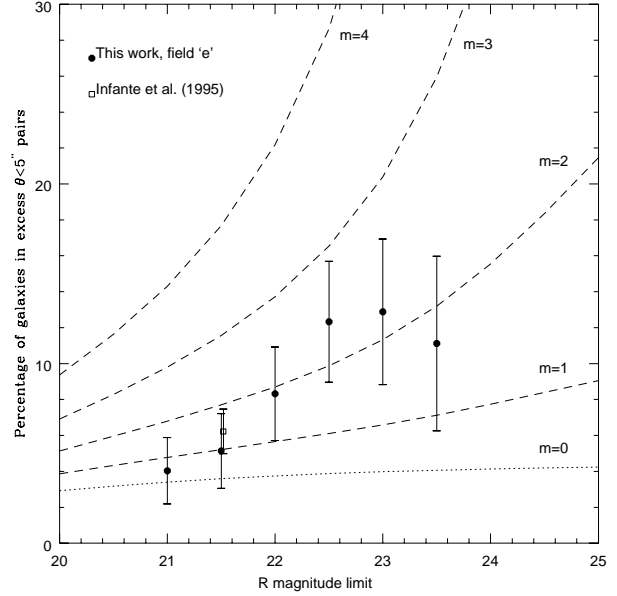


**Figure 8.** Fraction of galaxies in  $\theta < 5$  arcsec pairs in excess of the number expected by chance and the clustering observed at  $\theta > 5$  arcsec, as a function of  $R$  magnitude limit, from our field ‘e’ and from Infante et al. (1996). The dotted line shows a model in which the local fraction of galaxies in close pairs remains constant, the dashed lines are models in which the merger rate evolves as  $(1+z)^m$ , where  $m = 1, 2, 3, 4$ .

$$\mu_J = \frac{1}{m} \sum_{i=1}^m (N_i - \bar{N})^J. \quad (19)$$

and the second moment (variance) of the counts-in-cells will be related to  $\omega(\theta)$  as

$$\mu_2 = \bar{N} + \bar{N}^2 \int \int_{cell} \omega(\theta) d\Omega_1 d\Omega_2 \quad (20)$$

where the double integral is over the area of one cell. An area-averaged  $\omega(\theta)$ ,  $\bar{\omega}_2$ , can be defined as

$$\bar{\omega}_2 = \int \int \omega(\theta) d\Omega_1 d\Omega_2 \quad (21)$$

and estimated from the measured second moment by subtracting the expectation for a Poisson distribution (i.e.  $\mu_2 = \bar{N}$ ) and dividing by  $\bar{N}^2$ .

$$\bar{\omega}_2 = \frac{1}{\bar{N}^2} (\mu_2 - \bar{N}) \quad (22)$$

Similarly, the area-averaged angular three-point correlation function  $\bar{\omega}_3$  can be calculated from the excess of the third moment (skewness) relative to the Poisson expectation (see Baugh, Gaztañaga and Efstathiou 1995)

$$\bar{\omega}_3 = \frac{1}{\bar{N}^3} (\mu_3 - 3\mu_2 + 2\bar{N}) \quad (23)$$

and the area-averaged angular four-point correlation function  $\bar{\omega}_4$  can be calculated from the excess of the fourth moment (kurtosis) relative to the Poisson expectation

$$\bar{\omega}_4 = \frac{1}{\bar{N}^4} (\mu_4 - 3\mu_2^2 + 11\mu_2 + 6\bar{N}) \quad (24)$$

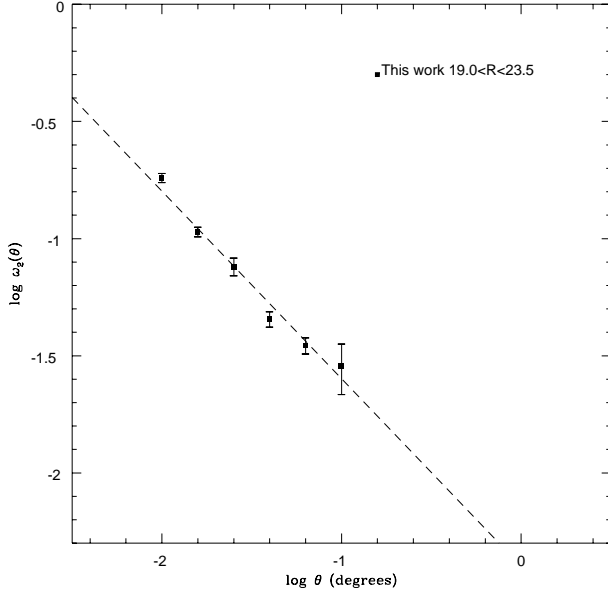


**Figure 9.** The area-averaged angular correlation function  $\bar{\omega}_2(\theta)$ , from the counts-in-cells analysis, with best-fit  $\theta^{-0.8}$  power-law

It is useful to express higher order correlation functions in the form of hierarchical amplitudes  $s_J$ , defined as

$$s_J = \frac{\bar{\omega}_J}{\bar{\omega}_2^{J-1}} \quad (25)$$

The hierarchical amplitudes depend much less on cell size than the  $\bar{\omega}_J$ , so are particularly suited to comparing shallow and deep surveys. We divide both field ‘e’ and ‘f’ into square cells of side  $\theta$ , and count the number of  $19 \leq R \leq 23.5$  galaxies in each cell. Many of the cells will overlap with field edges or holed areas. If the missing proportion of the cell area  $f_m$  was less than 0.3, the galaxy count was corrected by multiplying by  $(1 - f_m)^{-1}$ , while cells with  $f_m > 0.3$  were excluded from the analysis (as in Gaztañaga 1994). Combining fields ‘e’ and ‘f’, we calculate the variance, skewness and kurtosis of the counts-in-cells, and from these estimate  $\bar{\omega}_2$ ,  $s_3$  and  $s_4$  using equations 22–24. The analysis was repeated for cell size  $\theta$  ranging from 0.01 to 0.1 degrees.

Figures 9, 10 and 11 show these three functions as a function of cell size  $\theta$ . Error bars were calculated by randomly dividing the cells into 10 subsamples, calculating  $\bar{\omega}_2$ ,  $s_3$  and  $s_4$  for each subsample and dividing the scatter in the subsample amplitudes by  $\sqrt{10}$ .

For a  $\omega(\theta) = A\theta^{-0.8}$  power-law in square cells of side  $\theta$ , equation 20 gives  $\bar{\omega}_2(\theta) = 2.24A\theta^{-0.8}$ . The form of  $\bar{\omega}_2(\theta)$  is well-fitted by a  $\theta^{-0.8}$  power-law (Figure 11), with amplitude of  $40.0 \pm 0.9 \times 10^{-4}$  at one degree. Dividing by 2.24, this corresponds to a  $\omega(\theta)$  amplitude of  $A = 17.86 \pm 0.4 \times 10^{-4}$ . We estimate the star contamination for this sample as  $f_{\text{star}} = 0.154$ , giving an amplitude corrected for star contamination  $A = 24.94 \pm 0.6 \times 10^{-4}$ . This is slightly higher than but reasonably consistent with the amplitudes calculated from the positions of individual galaxies (Table 3), which despite their larger error bars will be more reliable.

Figures 12 and 13 show our  $s_3(\theta)$  and  $s_4(\theta)$  compared with the estimates from the two  $17 < B < 20$  surveys.

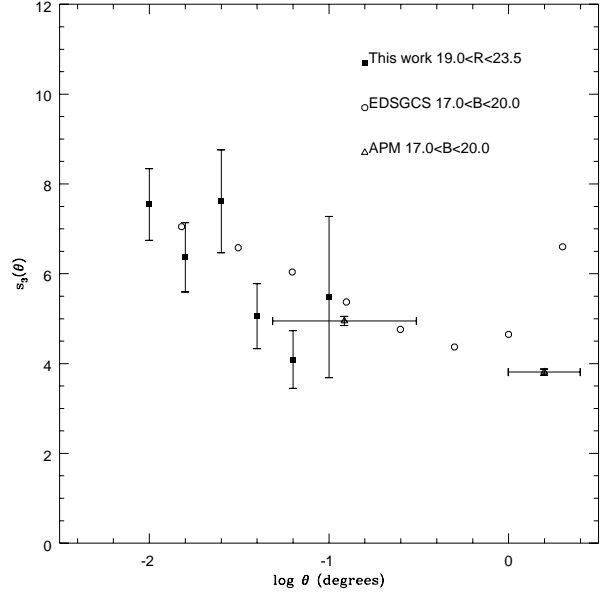


**Figure 10.** The hierarchical moment  $s_3(\theta)$  from our data, compared with  $s_3$  for brighter galaxies in the APM (Gaztañaga 1994) and EDSCGS (Szapudi et al. 1996) surveys.

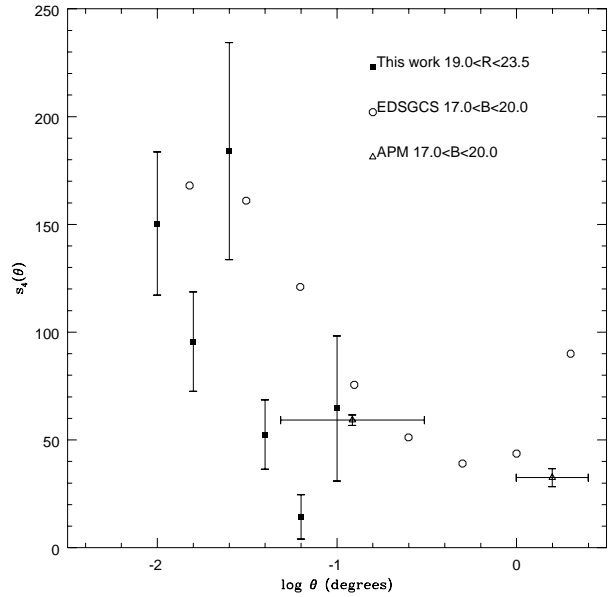


**Figure 11.** The hierarchical moment  $s_4(\theta)$  from our data, compared with  $s_4$  for brighter galaxies in the APM (Gaztañaga 1994) and EDSCGS (Szapudi et al. 1996) surveys.

Gaztañaga (1994) give  $s_3$  and  $s_4$  as mean values at  $0.05 \leq \theta \leq 0.3^\circ$  and at  $\theta > 1^\circ$ , whereas Szapudi et al. (1996) give amplitudes for 8 cell sizes from 0.015125 to 2.0 degrees.

The hierarchical amplitude  $s_3$  shows a very shallow slope with  $\theta$ , similar to that seen at  $B \leq 20$ . The mean amplitude at  $0.01 \leq \theta \leq 0.1$  degrees is  $6.42 \pm 0.47$ . Star

contamination will reduce  $\bar{\omega}_3$  by a factor  $(1 - f_{star})^{-3}$  but reduces the denominator  $\bar{\omega}_2^2$  by  $(1 - f_{star})^{-4}$ , so to correct for star contamination we multiply by  $(1 - f_{star})$  giving  $s_3 = 5.43 \pm 0.40$ .

At the mean redshift of these galaxies,  $z = 0.69$ , the angular diameter distance  $d_A = 956 h^{-1}$  Mpc compared to  $d_A = 380 h^{-1}$  Mpc for the APM galaxies, so it seems reasonable to compare our  $0.01 \leq \theta \leq 0.1$  degree estimate with the Gaztañaga (1994)  $0.05 \leq \theta \leq 0.3$  degree estimate and an average of the Szapudi et al. (1996) estimates at  $0.03125 \leq \theta \leq 0.5$  deg. At these angles, the APM and EDSGCS estimates at these angles are  $4.95 \pm 0.1$  and  $5.42$  respectively, the small difference between the two thought to be due to better sampling in the EDSGCS. As our result lies between these estimates, we conclude that there is no significant change in  $s_3$  between  $B \leq 20$  and  $R \leq 23.5$  limits. Within our  $2\sigma$  errors there could only be a  $\sim \pm 15\%$  change.

The hierarchical amplitude  $s_4$  shows a steeper decrease with  $\theta$ , as did that from the  $B \leq 20$  surveys. The mean amplitude at  $0.01 \leq \theta \leq 0.1$  degrees is  $83.7 \pm 32.5$ . Star contamination will reduce  $\bar{\omega}_4$  by a factor  $(1 - f_{star})^{-4}$  but reduces  $\bar{\omega}_2^3$  by  $(1 - f_{star})^{-6}$ , so to correct for star contamination we must multiply  $s_4$  by  $(1 - f_{star})^2$  giving a mean  $s_4 = 59.9 \pm 23.3$ . This compares to  $59.2 \pm 2.4$  in the APM survey at  $0.05 \leq \theta \leq 0.3$  deg and  $89.6$  for the EDSGCS at  $0.03125 \leq \theta \leq 0.5$  deg. Again, there is no evidence of significant evolution from  $B \leq 20$  to  $R \leq 23.5$ , but we can only set  $\sim \pm 70\%$  limits on this. As the error bars are much larger for this higher order correlation, we have not attempted to investigate  $s_5$  etc.

## 9 DISCUSSION

### 9.1 Clustering Evolution

Using a large sample of  $\sim 70000$  galaxies on two fields, we have measured the angular correlation function to a magnitude limit of  $R = 23.5$ . Field ‘f’ appears to have been badly chosen, the low Galactic latitude resulting in heavy star contamination and some extinction, although after corrections are applied for these effects the  $\omega(\theta)$  amplitudes are consistent with those from field ‘e’. Our results support the relatively high normalization of  $\omega(\theta)$  from the Infante and Pritchett (1995) and Woods and Fahlman (1997) surveys. These two surveys used very high Galactic latitude fields, minimizing star-contamination, so may be the most reliable of previous  $\omega(\theta)$  estimates in this magnitude range.

We can also compare our results with  $\omega(\theta)$  amplitudes measured in other passbands at limits with a similar surface density of galaxies. Our  $\omega(\theta)$  amplitudes at  $R \sim 22.5\text{--}23.5$  are similar to those measured at  $I \sim 22\text{--}24$  (Neuschaefer et al. 1995; Brainerd and Smail 1998) and  $K \sim 19.5\text{--}21.5$  (Carlberg et al. 1997; Roche et al. 1998b) but higher than at limits of  $B \sim 24.5$  (Roche et al. 1993) and  $V \sim 24.5$  (Woods and Fahlman 1997). This would be expected from the observed dependence of  $\omega(\theta)$  amplitude on  $V - I$  (Neuschaefer et al. 1995)  $B - R$  (Roche et al. 1996) and  $U - K$  (Carlberg et al. 1997).

Neuschaefer et al. (1997) find the  $\omega(\theta)$  amplitude of bulge-profile galaxies at  $I \leq 23$  to be 2–4 times higher than that of disk galaxies, indicating that the colour dependence

is due at least in part to stronger clustering of earlier Hubble types, as observed locally (e.g. LMEP, Guzzo et al. 1997), and that this morphological segregation is maintained to at least  $z \sim 0.7$ . This would explain why the change in  $\omega(\theta)$  with wavelength appears greatest between the  $R$  and  $V$  passbands, as these would lie on either side of the  $4000\text{\AA}$  break for galaxies near the peak of  $N(z)$  and the size of this break correlates strongly with Hubble type.

Our results are consistent with the strength of galaxy clustering measured locally (LMEP), combined with galaxy  $L^*$  evolution consistent with current redshift surveys, and galaxy clustering approximately stable ( $\epsilon = 0$ ) in proper co-ordinates. For the  $N(z)$  and  $r_0$  of our model, the best fitting clustering evolution is  $\epsilon = -0.03 \pm 0.44$ . Strong clustering evolution of  $\epsilon = 1.2$  is disfavoured by  $\sim 3\sigma$ , as is comoving clustering ( $\epsilon = -1.2$ ). Our estimate of  $\epsilon$  can be compared with the simulations of Colín et al. (1997), which for the clustering of the matter distribution predict  $\epsilon = 1.08 \pm 0.09$  for  $\Omega = 1$  and  $\epsilon = 0.18 \pm 0.12$  for  $\Omega = 0.2$ .

On the face of it, the observations appear to strongly favour a low density Universe. However, the situation is more complicated if the galaxy luminosity distribution is strongly biased relative to the fluctuations in the density field. An extreme example of biasing is the ‘merging model’ of Matarrese et al. (1997), in which visible galaxies are identified with very massive ( $\sim 10^{13} h^{-1} M_\odot$ ) dark matter halos, with a linear bias ( $b$ ) relative to mass fluctuations of  $b = 1.46$  at  $z = 0$  and evolving as  $b = 0.41 + 1.05(1+z)^{1.8}$ . As  $\xi(r) \propto b^2$ , this biasing would increase  $\xi(r)$  by a factor 7.76 at  $z = 1$ , corresponding to  $\epsilon_{galaxies} \simeq \epsilon_{mass} - 3$ . Not surprisingly, such a model overpredicted the observed faint galaxy  $\omega(\theta)$  and could be rejected, in any cosmology (Moscardini et al. 1998).

Matarrese et al. (1997) also present a ‘transient model’ in which star-forming faint galaxies are identified with less massive ( $\sim 10^{11} h^{-1} M_\odot$ ) halos and are assumed to evolve into a weakly clustered ( $b = 0.67$  hence  $r_0 \simeq 2 h^{-1}$  Mpc), low surface brightness population at the present day (see also Efstathiou 1995). The bias again evolves rapidly as  $b = 0.41 + 0.26(1+z)^{1.85}$ , which at  $z \sim 1$  results in clustering similar to present day galaxies with  $\epsilon \sim 0$ . For a  $z < 1.6$  sample (approximately the depth of our data) the transient model  $\omega(\theta)$  is indistinguishable from an unbiased ( $b = 1$ ) model, so our  $\omega(\theta)$  results would not be able to exclude it. However, there may be further constraints on galaxy biasing from other statistics such as the higher-order correlation functions (Section 9.3).

Limits on clustering evolution from this data will only apply to  $z \sim 1.5$ , as few higher redshift galaxies will be detected (Figure 8). However, Giavalisco et al. (1998) recently measured  $\omega(\theta)$  for a sample of photometrically-selected Lyman-break galaxies at  $z_{mean} = 3.04$ , estimating a comoving correlation length of  $r_0 = 3.3^{+0.7}_{-0.6} h^{-1}$  Mpc, corresponding to  $r_0 = 0.82^{+0.17}_{-0.15} h^{-1}$  Mpc in proper co-ordinates. This would be related to the present-day correlation radius  $r_0(z = 0)$  as

$$r_0^\gamma = [r_0(z = 0)]^\gamma (1 + z)^{-(3+\epsilon)} \quad (26)$$

It is uncertain whether the present-day counterparts of these galaxies will be predominantly ellipticals or spirals (in our model  $f_e \sim 0.33$  at this redshift), but for any mixture the present day correlation radius will be in the  $4.2 \leq r_0(z = 0) \leq 8.4 h^{-1}$  Mpc range, which with  $\gamma = 1.8$



requires a clustering evolution from  $z = 0$  to  $z \sim 3$  in the range  $-0.9 \leq \epsilon \leq 0.0$ . Hence there may be some indication that the clustering increases a little above the stable model at these high redshifts, presumably due to an increase in the linear bias, but this is a very moderate effect in comparison to the Matarrese et al. (1997) merging model. The low  $\omega(\theta)$  amplitude of the Hubble Deep Field sample as a whole suggests that  $\epsilon$  would only become significantly negative at the highest ( $z \gtrsim 2$ ) redshifts.

Villumsen et al. (1997) originally interpreted the low  $\omega(\theta)$  amplitudes on the Hubble Deep Field as favouring  $r_0 \simeq 4 h^{-1}$  Mpc locally with  $\epsilon = 0.8$  clustering evolution. Although we may not be able to strongly exclude  $\epsilon = 0.8$ , our data and the  $z \sim 3$  clustering measured by Giavalisco et al. (1998) both suggest that  $\epsilon$  is closer to zero. Furthermore, faintward of  $R \sim 26$ , it is unlikely that  $N(z)$  will become much more extended, and the most important change in  $N(z)$  is that less luminous galaxies are seen in the same volume of space. It therefore seems more likely that any further decrease in  $\omega(\theta)$  amplitude at  $R > 26$  is primarily due to a decrease in  $r_0$  at low luminosities rather than clustering evolution. This interpretation would be supported by the results of Connolly, Szalay and Brunner (1998) - who divided the Hubble Deep Field galaxies at  $I \leq 27$  (where dwarfs will dominate the sample) by photometric redshift and found weak intrinsic clustering of  $r_0 = 2.37 h^{-1}$  Mpc over the  $0.4 < z < 1.6$  range, with  $\epsilon = -0.4^{+0.37}_{-0.65}$  consistent with stable clustering.

We find no evidence a flattening of the slope of  $\omega(\theta)$  on going faintward (Table 4). Giavalisco et al. (1998) estimate a  $\omega(\theta)$  slope  $\delta = 0.98^{+0.32}_{-0.28}$  for  $z \sim 3$  galaxies, which at least suggests that the relatively steep slope in our data is maintained to much higher redshifts. The flattening reported by Infante and Pritchet (1995) might then be at least in part caused by sensitivity gradients near the limits of photographic data. None of our calculated  $\omega(\theta)$  are significantly flatter than  $\delta = 0.8$ , at any magnitude limit, which suggests that the  $\xi(r)$  of spiral galaxies, which would form the greater part of our catalog, is close to  $\gamma = 1.8$ , and certainly no flatter than the  $\gamma = 1.72$  of LMEP.

A constant slope for  $\omega(\theta)$  may not be surprising, as the Colín et al. (1997) simulations predict no significant flattening of the  $\xi(r)$  of the mass distribution, even to  $z \sim 5$ , for any  $\Omega$ . They do predict some flattening ( $\Delta(\gamma) \simeq -0.2$  to  $z \sim 1$ ) of the galaxy  $\xi(r)$  for a strongly biased model, but such models already seem disfavoured by the  $\omega(\theta)$  scaling. Some flattening of  $\omega(\theta)$  between  $R = 21$  and  $R = 23.5$  might be expected from the decrease in the fraction of ellipticals (Figure 9b), but we estimate that this would only amount to  $\Delta(\delta) \simeq -0.02$  to  $-0.04$  (from the LMEP and Guzzo et al.  $\gamma$  respectively). This would be less than the  $1\sigma$  errors in our estimates of  $\delta$  (Table 4), so might still be consistent with our results. Alternatively, this effect might be entirely cancelled out by the increase on going faintward in the fraction of lower luminosity galaxies (Figure 9b), as these may also have a steeper  $\xi(r)$  than  $L^*$  spirals - LMEP estimate  $\gamma = 2.01 \pm 0.1$  for late-type galaxies with  $M_B > -20.5$ .

Further investigation of the evolution of the amplitude and slope of  $\omega(\theta)$  will simply require large-format CCD surveys of a similar area to greater depths. The differences between the results from our two fields suggests future surveys of this type should be confined to Galactic latitudes above

$\sim 45^\circ$ . Deep imaging in more than one passband will allow the  $\omega(\theta)$  of different galaxy types to be studied separately, and ultimately, a division of the galaxies by both Hubble type and photometric redshift.

## 9.2 Merger Rate Evolution

On the larger of our two fields, we find an excess of up to  $3.6\sigma$  significance in  $\omega(\theta)$  at  $2 \leq \theta \leq 5$  arcsec compared to the  $\theta^{-0.8}$  power-law fitted at  $\theta > 5$  arcsec. This was interpreted in terms of the fraction of the total sample of galaxies within  $\theta < 5$  arcsec pairs in excess of the expectation from chance and from the clustering seen at larger separations. The excess pair fraction was consistent with Infante et al. (1996) at  $R \leq 21.5$ , and suggested some further increase between  $R = 21.5$  and  $R = 23.0$  limits. The evolution in the pair fraction will follow approximately the evolution of the merger rate, parameterized here as  $R_m = R_{m0}(1+z)^m$ .

By comparing the fraction of galaxies in close pairs at  $V \leq 22.5$  with that at very low redshifts, Carlberg et al. (1994) claimed rapid evolution of  $m = 3.4 \pm 1.0$ , but this was based on a very small sample. With a dataset  $\sim 40$  times larger, Infante et al. (1996) estimated a merger rate evolution of  $m = 2.2 \pm 0.5$  at  $R \leq 21.5$ . Roche et al. (1998a) found marginal evidence for an excess of close pairs at a limit of  $K \leq 20$ , corresponding to  $m \simeq 2.1^{+0.8}_{-1.3}$ . Modelling the pair fraction as a function of  $R$  limit, we estimated  $m = 1.65^{+0.62}_{-0.88}$  for our field 'e' data to  $R = 23.0$ . This estimate of  $m$  must be viewed with some caution in view of the lack of a significant excess of close pairs on field 'f', presumably related to poorer seeing. The difference in the close pair counts between the Redeye and Magic data of Roche et al. (1998b) might support this interpretation, but the discrepancy may only be resolved by further  $> 1 \text{ deg}^2$  surveys in much better observing conditions. Neuschaefer et al. (1997) derived an even lower rate of  $m = 1.2 \pm 0.4$  from the close pair fraction on deep ( $I \leq 25$ ), after taking into account  $\theta^{-0.8}$  clustering.

The above estimates of the merger rate evolution appear reasonably consistent with the  $m \simeq 2$  expected for a low density Universe, and seem to reject the  $m \simeq 4$  expected for  $\Omega = 1$  (Carlberg et al. 1994). Comparing our results with the shallower Infante et al. (1996) and the deeper Neuschaefer et al. (1997) data, there might also be hints of a reduction in  $m$  with increasing survey depth. This might be expected if merging leads to even a moderate reduction in mean galaxy mass at high redshifts. Carlberg et al. (1994) predict that  $m$  will depend on  $\Omega$  as  $m \simeq 4.51\Omega^{0.42}$ , changing to  $m \simeq 3.2\Omega^{0.57}$  if the mean galaxy mass is reduced by 32%. Hence if, for example,  $\Omega = 0.2$  and the mean mass falls by  $\sim 32\%$  at the  $z \sim 2$  depth of the  $I \leq 25$  data, this would give  $m \simeq 2.29$  at low redshift falling to  $m \simeq 1.28$  for the Neuschaefer et al. (1997) data, in agreement with observations. Larger amounts of deep, high resolution data will obviously be needed to confirm this.

## 9.3 Hierarchical Moments and Non-linear Bias

Using a simple counts-in-cells method, we investigated the area-averaged three and four point correlation functions of the  $R < 23.5$  galaxies, giving the results in the form of the hierarchical moments  $s_3(\theta)$  and  $s_4(\theta)$ . A positive  $s_3(\theta)$

was detected with high ( $\sim 10\sigma$ ) significance, although the detection of  $s_4(\theta)$  was much weaker. We find that that  $s_3(\theta)$  and  $s_4(\theta)$  show no significant evolution between  $B = 20$  and  $R = 23.5$  limits, with evolution of  $s_3(\theta)$  constrained to  $\lesssim \pm 15\%$ .

For a distribution of mass  $\rho_{mass}(\mathbf{r})$ , with fluctuations about the mean  $\delta_{mass}(\mathbf{r}) = \rho_{mass}(\mathbf{r}) - \langle \rho_{mass} \rangle$ , and a distribution of the galaxy luminosity in a particular passband  $\rho_{gal}(\mathbf{r})$ , with fluctuations  $\delta_{gal}(\mathbf{r}) = \rho_{gal}(\mathbf{r}) - \langle \rho_{gal} \rangle$ , the biasing of galaxies relative to mass can be expressed as the series (e.g. Fry and Gaztañaga 1993)

$$\delta_{gal}(\mathbf{r}) = \sum_{k=0}^{\infty} \frac{b_k}{k!} \delta_{mass}(\mathbf{r}) \quad (27)$$

The galaxy  $\xi(r)$  can be interpreted as the  $\xi(r)$  of the underlying mass distribution multiplied by  $b_1^2$ , where  $b_1$  is the linear bias. The hierarchical moments of the galaxy distribution are related to those of the mass distribution through expressions involving the higher-order (non-linear) bias coefficients,

$$s_{3(gal)} = (s_{3(mass)} + 3 \frac{b_2}{b_1})/b_1 \quad (28)$$

$$s_{4(gal)} = (s_{4(mass)} + 12 \frac{b_2}{b_1} s_{3(mass)} + 4 \frac{b_3}{b_1} + 12 \frac{b_2^2}{b_1^2})/b_1^2 \quad (29)$$

Gaztañaga (1994) found the APM survey hierarchical moments to be consistent with those of the mass distribution in  $N$ -body simulations of evolution under gravity, with the best-fit for a low density CDM model (Gaztañaga and Frieman 1994). This implied a simple model in which blue-band luminosity from galaxies linearly traces the mass, with  $b_1 \simeq 1$  (upper limit  $b_1 < 1.15$ ) and  $b_k \simeq 0$  for all  $k > 1$ . In contrast, IRAS galaxies, which are less clustered than optically selected galaxies (implying  $b_{1(IRAS)} \simeq 0.7$ ), also give  $s_3(\theta)$  a factor 2 lower and  $s_4(\theta)$  a factor 3 lower than optically-selected galaxies. This indicates a non-linear bias with a negative  $b_2$ , so that IRAS galaxies are biased away from rich clusters.

Simulations (Gaztañaga and Baugh 1995) predict that the  $s_J$  of the underlying mass distribution will not change significantly with time, even over three expansion factors of the Universe. Any change in the  $s_J$  between a shallow and deep survey would therefore indicate a change in the biasing of luminosity relative to mass. Our results show, with as much as  $\sim 6\sigma$  significance, the biasing properties of  $R \leq 23.5$  galaxies to be more similar to nearby blue-selected galaxies than to IRAS galaxies. As the  $R$ -band corresponds approximately to rest-frame blue near the mean redshift, this indicates that the rest-frame blue-band continues to linearly trace the mass density distribution out to  $z \sim 1$ .

If biasing properties are approximately constant to the depths of our survey, the  $\omega(\theta)$  scaling indicates  $\epsilon \simeq 0$  for the mass distribution as well as the galaxies. At this point many of our results (the stability of clustering, the mild evolution of the merger rate, the lack of evidence for a transient population) appear to favour a low  $\Omega$  cosmology. Strongly biased models (e.g. Matarrese et al. 1996; Moscardini et al. 1998) could no doubt be adjusted to fit the  $\omega(\theta)$  scaling for a wide range of cosmological models, but higher-order correlation functions may have the potential to break the apparent de-

generacy between the biasing model and the cosmological model.

In the absence of detailed models, our tentative interpretation is that this result is as expected for PLE type evolution – in which ellipticals and spirals, and dwarf and giant galaxies, would all undergo a similar evolutionary brightening over this redshift range – but would argue against ‘transient’ or ‘disappearing dwarf’ models (e.g. Babul and Rees 1992), in which a large proportion of the faint blue galaxies are low mass systems undergoing brief starbursts. (eg. Efstathiou et al. 1995). Although the ‘transient model’ of Matarrese et al. (1996) is consistent with the  $\omega(\theta)$  at this depth, such models are likely to underpredict the hierarchical moments, as the transient dwarfs are associated with low mass haloes collapsing at relatively late epochs. These are expected to have a negative  $b_2$  (Mo and White 1996) and to produce a much lower  $s_3$  and  $s_4$  than the mass distribution or the APM/EDSGCS galaxies, even if their linear bias is greater than unity (Mo, Jing and White 1997).

As larger areas are surveyed, the estimation of hierarchical moments  $s_3(\theta)$  and  $s_4(\theta)$  is likely to become an important complement to the study of the faint galaxy  $\omega(\theta)$ . The investigation of even higher order moments would seem to require samples of several  $\times 10^5$  galaxies, like the APM and EDSCS surveys. Further investigations would involve surveying a similar area to a greater depth, and in more than one passband. Colour data could help to verify the above conclusions by allowing the hierarchical moments of the blue star-forming galaxies to be studied out to high redshifts without ‘contamination’ from the more strongly clustered red ellipticals.

## 10 SUMMARY OF MAIN CONCLUSIONS

- (i) On two areas of sky totalling  $1.75 \text{ deg}^2$ , we measure galaxy  $\omega(\theta)$  amplitudes at limits from  $R = 21$  to  $R = 23.5$ . After correction for star contamination, our  $\omega(\theta)$  amplitudes are consistent with previous surveys and support the relatively high normalization of the Infante and Pritchet (1995) and Woods and Fahlman (1997)  $\omega(\theta)$  scaling.
- (ii) Assuming the redshift distribution from our PLE model and present-day correlation radii from Loveday et al. (1995), our results are most consistent with galaxy clustering approximately stable in proper co-ordinates ( $\epsilon = -0.03 \pm 0.44$ ). This suggests that the low  $\omega(\theta)$  amplitude of fainter galaxies (e.g. on the Hubble Deep Field) is the result of weaker clustering of dwarfs rather than clustering evolution.
- (iii) The slope of the  $\omega(\theta)$  power-law is  $\delta \simeq 0.8$  and shows no significant flattening on going faintward.
- (iv) On the larger of our fields, the amplitude of  $\omega(\theta)$  is higher at  $2 \leq \theta \leq 5 \text{ arcsec}$  than at  $\theta > 5 \text{ arcsec}$ . The proportion of the galaxies in the excess  $\theta < 5 \text{ arcsec}$  pairs is consistent with the local fraction of galaxies in close pairs, combined with a merger/interaction rate evolving as  $(1+z)^m$ , where  $m = 1.65^{+0.62}_{-0.88}$ .
- (v) The hierarchical moments  $s_3(\theta)$  and  $s_4(\theta)$ , estimated from the counts-in-cells of the  $19 \leq R \leq 23.5$  galaxies, are similar to those measured for  $17 \leq B \leq 20$  galaxies in the APM and EDSCS surveys. This implies that the rest-frame blue-band luminosity from galaxies continues to trace the underlying mass distribution, without strong linear or

non-linear biasing, out to  $z \sim 1$ . This disfavors ‘transient’ models and supports the interpretation of the stable galaxy clustering as evidence for an unbiased low  $\Omega$  Universe.

### Acknowledgements

The Isaac Newton Telescope is operated on the island of La Palma by the Isaac Newton Group in the Spanish Observatorio del Roque de los Muchachos of the Instituto de Astrofísica de Canarias. The data reduction and analysis were carried out at the University of Wales Cardiff, using facilities provided by the UK Starlink project, funded by the PPARC. Nathan Roche acknowledges the support of a PPARC research associateship.

### REFERENCES

- Babul A., Rees M. J., 1992, MNRAS, 255, 346.  
Bahcall J. N., Soneira R. M., 1980, ApJS 44, 73.  
Baugh C. M., Gaztañaga, E., Efstathiou, G., 1995, MNRAS 274, 1049.  
Bershady M., Majewski S., Koo D. C., Kron R. G., Munn J. A., 1997, ApJ, L41.  
Brainerd T. G., Smail I., Mould, J. R., 1995, MNRAS, 275, 781.  
Burstein D., Heiles C., 1978, ApJ, 225, 40.  
Carlberg R. G., Cowie L. L., Songaila A., Hu E. M., 1997, ApJ, 484, 538.  
Carlberg R. G., Pritchett C. J., Infante L., 1994, ApJ, 435, 540.  
Charlot S., Worthey G., Bressan A., 1996, ApJ, 457, 625.  
Colín P., Carlberg R. G., Couchman H. M. P., 1997, ApJ, 490, 1.  
Connolly A.J., Szalay A.S., Brunner R.J., 1998, ApJ, submitted.  
Couch W. J., Jurcèvic J. S., Boyle B. J., 1993, MNRAS, 260, 241.  
Cowie L. L., Songaila A., Hu, E. M., 1996, AJ, 112, 839.  
Efstathiou G., 1995, MNRAS, 272, L25.  
Efstathiou G., Bernstein G., Katz N., Tyson J.A., Guhathakurta P., 1991, ApJ, 380, L47.  
Fry J. N., Gaztañaga, E. 1993, ApJ, 413, 447.  
Gaztañaga E., 1994, MNRAS, 268, 913.  
Gaztañaga E., Baugh C. M., 1995, MNRAS, 273, L1.  
Gaztañaga E., Frieman J., 1994, ApJ, 437, L13.  
Gialvalisco M., Steidel C. C., Adelberger K. L., Dickinson M., Pettini M., Kellogg M., 1998, ApJ, submitted.  
Groth E. J., Peebles P. J. E., 1977, ApJ, 217, 385.  
Guzzo L., Strauss M. A., Fisher K., Giovanelli R., Haynes M., 1997, ApJ, 489, 37.  
Infante L., de Mello D. F., Menanteau, F., 1996, ApJ, 469, L85.  
Infante L., Pritchett C.J., 1995, ApJ, 439, 565.  
Landolt A. U., 1992, AJ, 104, 340.  
Le Fèvre O., Hudon D., Lilly S. J., Crampton D., Hammer F., Tressè L., 1996, ApJ, 461, 534.  
Loveday J., Maddox S. J., Efstathiou G., Peterson B. A., 1995, ApJ, 442, 457.  
Madau P., Ferguson H., Dickinson M., Gialvalisco M., Steidel C., Fruchter A., 1996, MNRAS, 283, 1388.  
Maddox S. J., Efstathiou G., Sutherland W. J., Loveday J., 1990, MNRAS, 242, L43.  
Marzke R. O., Geller M. J., Huchra J. P., Corwin H. G. Jr., 1994, AJ, 108, 437.  
Matarrese S., Coles P., Luccin F., Moscardini L., 1996, MNRAS 286, 115.  
Mathis J., 1990, A&A Ann. Rev, 38, 37.  
Metcalf N., Shanks T., Fong R., Jones L., 1991, MNRAS, 249, 498.  
Metcalf N., Shanks T., Fong R., Roche N., 1995, MNRAS, 273, 257.  
Mihos J. C., Hernquist L., 1996, ApJ, 464, 641.  
Mo, H. J., Jing Y. P., White, S.D.M., 1997, MNRAS 284, 189.  
Mo, H. J., White, S.D.M., 1996, MNRAS 282, 347.  
Moscardini L., Coles P., Lucchin F., Matarrese S., 1998, MNRAS, in press.  
Neuschaefer L. W., Ratnatunga K., Griffiths R.E, Casertano S., 1995, ApJ, 453, 559.  
Neuschaefer L. W., Ratnatunga K., Griffiths R.E, Casertano S., 1997, ApJ, 480, 59.  
Phillipps S., Fong R., Ellis R. S., Fall S. M., MacGillivray H. T., 1978, MNRAS, 182, 673.  
Roche N., Eales S., Hippelein H., 1998b, MNRAS, in press.  
Roche N., Ratnatunga K., Griffiths R. E., Im M., Naim A., 1998a, MNRAS 293, 157.  
Roche N., Shanks T., Metcalfe N., Fong R., 1993, MNRAS, 263, 360.  
Roche N., Shanks T., Metcalfe, N., Fong R., 1996, MNRAS, 280, 397.  
Shepherd C. W., Carlberg R. G., Yee H. K. C., 1997, ApJ, 479, 82.  
Stark A., Gammie C., Wilson R., Bally J., Linke R., Heiles C., Hurwitz M., 1992, ApJS, 79, 77.  
Steidel C. C., Gialvalisco M., Dickinson M., Adelberger K. L., 1996, AJ, 112, 352.  
Szapudi I., Meiksin A., Nichol R., 1996, ApJ 473, 15.  
Villumsen J. V., Freudling W., da Costa, L., 1997, ApJ, 481, 578.  
Woods D., Fahlman, G., 1997, ApJ, 490, 11.